FREQUENCY SELECTIVE SURFACE TO ENHANCE THE PERFORMANCE OF HIGH FREQUENCY ANTENNA

BHARAT BISHT 071139
JAGMEET SINGH SANDHU 071141
KRISHNA KUMAR 071143

NAME OF SUPERVISOR DR.GHANSHYAM SINGH

May -2011

Submitted in partial fulfillment of the Degree of Bachelor of Technology

B.Tech

DEPARTMENT OF ELECTRONICS AND COMMUNICATION ENGINEERING

JAYPEE UNIVERSITY OF INFORMATION TECHNOLOGY,

WAKNAGHAT

TABLE OF CONTENTS

CERTIFICATE

This is to certify that the project report entitled "**Frequency selective surface to enhance the performance of high frequency antenna**", submitted by **Bharat Bisht, Jagmeet Singh Sandhu** and **Krishna Kumar** in partial fulfillment for the award of degree of Bachelor of Technology in Electronics and Communication Engineering to Jaypee University of Information Technology, Waknaghat, Solan has been carried out under my supervision. It is certified that this work has not been submitted partially or fully to any other University or Institute for the award of this or any other degree or diploma.

Signature of Supervisor

Name of Supervisor Dr. Ghanshyam Singh

Designation Associate professor

Date

ACKNOWLEDGMENT

As we conclude our project with the God's grace, we have many people to thank; for all the help, guidance and support they lent us, throughout the course of our endeavor.

First and foremost, we thank Dr Ghanshyam Singh, our Project Guide, who has always encouraged us to put in our best efforts and deliver a quality and professional output. His methodology of making the system strong from inside has taught us that output is not the end of project. We really thank him for his time & efforts.

Secondly, we thank Mr. Kumud Ranjan Jha(Asst. Professor, SMVDU, Jammu) and Ms Pragya Gupta, for their patient hearing of our ideas and opening up our minds to newer horizons by pointing out our flaws, providing critical comments and suggestions to improve the quality of our work and appreciating our efforts. We also want to thank Mr. Mohan Sharma for his consistent co-operation and providing us every required facility in the lab.

Apart from these, countless events, countless people & several incidents have made a contribution to this project that is indescribable.

(Bharat Bisht) (Jagmeet Singh Sandhu) (Krishna Kumar)

SUMMARY

In this project, we have simulated the dielectric rod antenna by using CST microwave studio which is commercially available simulator based on finite integral technique and we studied different types of FSS in CST. We emphasize particularly, on the gain of the proposed antenna at two frequencies that is from 25GHz to 35 GHz. The radiation mechanism of the dielectric rod antenna is based on the discontinuity radiation concept in which the antenna is regarded as an array composed of two effective sources at the feed end and free end of the rod. The dielectric rod antenna has a dielectrically filled circular waveguide section that serves as a feed for the dielectric rod. This is followed by a feed taper section that is mainly used for matching the feed to the dielectric rod. The main body of the antenna follows the feed taper and ends in a terminal taper. A frequency selective surface is a periodic array of either radiating or non-radiating elements or slots which effectively act as a bandstop or bandpass filter respectively to electromagnetic waves. The frequency selective surfaces (FSS) are periodic structures in either one or two dimensions (i.e. singly or doubly periodic structures) which perform a filter operation. Thus, depending on their physical construction, material and geometry, they are divided into low-pass, high-pass, band-pass and band-stop filters. FSS can be cascaded to form a triply-periodic structure which is commonly known as a photonic crystal. There are a wide variety of possible elements which can be used to realize FSS arrays as will be discussed later.

Bharat Bisht, 071139 **Dr. Ghanshyam Singh**

Jagmeet Singh Sandhu, 071141

Krishna Kumar, 071143

List of Figures page

List of Tables Page

Chapter 1
Introduction

1.1 Introduction

Since radio transmission was first demonstrated by Heinrich Hertz at the Technical Institute in Karlsruhe, Germany in 1886 and Guglielmo Marconni's success with transatlantic communication in the beginning of the 20th century, antennas have become an indispensable technology, linking people and places in ways that people could only dream of a century ago. Antennas have permeated into many aspects of our daily lives, and have enabled several advances in mankind's knowledge of both Earth and its inhabitants and the universe in which we live.

A wide variety of antennas are utilized for an array of applications, from weather and global positioning satellites to ground based antenna arrays which are used to receive extraterrestrial radio transmissions to antennas used in radios and cell phones. A multitude of antenna types exist, including monopole and dipole antennas, loop antennas, dish antennas, and horn antennas. These antennas can be arranged in arrays to realize high gain and directivity with several small antennas instead of one large antenna.

1.1.1 Introduction dielectric rod antenna

In this project we have studied about dielectric rod antenna, and about its various parameters like radiation pattern, gain, directivity's-parameters. A dielectric rod is an antenna which support HE_{11} hybrid mode. Inside the rod we describe the fields with Bessel function Jn. Outside the rod the fields fall off exponentially and we use the modified Bessel function Kn. The hybrid mode consists of the sum of TE_{11} and TM_{11} modes. The dielectric rod antenna is fed by circular waveguide supporting the TE11 mode, which excites the hybrid mode HE_{11} on the rod. At the waveguide exit we use a rod diameter as defined in later chapters. The second region of the rod tapers either to a uniform diameter section to produce discuss in later chapter on dielectric rod antenna. At the end of the antenna we taper the rod rapidly in a terminating section to bring the relative propagation constant of the surface wave near 1, to reduce reflection from the end. The dielectric antenna is used

1.1.2 Introduction of FSS

In this project we had studied about the frequency selective surfaces (FSS).Frequency selective surfaces is type of array which can be either radiating or non-radiating and is composed of a periodic array of elements or slots. Element and slot FSS arrays effectively create band stop and band pass filters respectively to electromagnetic energy at their design frequency range. These types of filters are used in a wide variety of applications, including radomes, dichroic surfaces, circuit analog absorbers and meander line polarizer.

Radomes are the protective cover placed in front of an antenna. For applications, such as military aircraft, these surfaces are designed such that the radar cross section (RCS) of a structure is minimized. Circuit analog absorbers are composed of a periodic array of resistive elements which when designed properly can achieve greater than 25 dB of attenuation over a decade of bandwidth (frequency ratio of 10:1.) Meanderline polarizers are used to transform linear polarization to circular polarization and vice versa over a bandwidth of up to an octave.

Various techniques in analyzing scattering from periodic structures have been developed over the past four decades. Few analyzing techniques are:

Method of Moments: The MoM is the most commonly used technique in analyzing scattering from an FSS This method evaluates the current flows on the conducting elements by matching the tangential field at the surface of the element and forming an integral equation for the unknown current. Analyses based on the MoM usually involve utilizing a periodic Green's function. Evaluations of the periodic Green's function and solving a large set of simultaneous linear equations can be computationally expensive.

Finite element method: An alternative approach for modeling the field scattered from a periodic structure is the finite element method (FEM) [48, 57{62]. FEM is a numerical procedure for obtaining solutions to boundary-value problems [63, p23].

FDTD: As opposed to the MoM and FEM approaches which analyze the periodic structure in the frequency-domain, FDTD is a time-domain technique, so the solution can cover a wide frequency range in a single simulation run. The FDTD approach is a direct solution of Maxwell's time dependent curl equations

Mutual impedance method: mutual impedance method to evaluate the field scattered from an FSS. This method determines the voltage induced by the incident wave at the element and also the mutual impedance between elements. Current flows on the element can hence be verified.

Equivalent Circuit Model: In contrast to the above computationally intensive approaches, the EC model offers a simpler alternative method in FSS analyses. Based on a transmission line analogy, transmission characteristics of an FSS structure can be determined.
In this we had studied FSS using equivalent circuit model which we will discuss in later chapters.

Chapter 2

Overview of Frequency Selective Surfaces

2.1 Introduction

A frequency selective surface is a periodic array of either radiating or non-radiating elements or slots which effectively act as a band stop or band pass filter respectively to electromagnetic waves. The frequency selective surfaces (FSS) are periodic structures in either one or two dimensions (i.e. singly or doubly periodic structures) which perform a filter operation. Thus, depending on their physical construction, material and geometry, they are divided into low-pass, high-pass, band-pass and band-stop filters. As can be seen in Fig 2.1 the FSS can be cascaded to form a triply-periodic structure which is commonly known as a photonic crystal. There are a wide variety of possible elements which can be used to realize FSS arrays as will be discussed in later in this section.

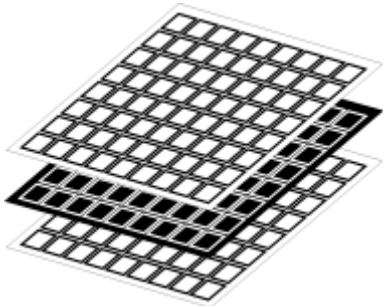

Figure: 2.1 FSS

2.2 History of FSS

The FSS were intensively studied since the 1960s [12] although as early as 1919Marconi patented such periodic structures [3]. From 1969 until the end of 2000, more than 200 papers were published containing the keyword "frequency selective surface"(INSPEC Catalogue search 12/1/2001). Early work concentrated on the use of FSS in Cassegainian sub reflectors in parabolic dish antennas. FSS are now employed in radomes (terrestrial and airborne), missiles and electromagnetic shielding applications. The analysis of FSS started with mode matching techniques which were first applied to aperture problems. In addition, the mode matching

method led to the approximate method of equivalent circuit analysis which gave some insight into the behavior and design of FSS. With the advent of computers more accurate numerical techniques were developed for the analysis of FSS. The techniques used in the mode matching method which initially was applied to solve aperture type FSS problems, were employed to solve patch problems. Other powerful numerical methods such as the finite difference time domain method and the finite element method were also employed to solve FSS problems. Experiments are necessary to verify the performance of practical FSS structures, confirm the accuracy of theoretical/numerical predictions and provide results for FSS structures which are difficult to simulate.

2.3 FSS and its applications

Frequency Selective surfaces (FSSs) are planar periodic structures that behave like filters to electromagnetic energy. The surface is assembled with identical patch or aperture conducting elements repeating periodically in either a one- or two-dimensional array [1, 3]. Based on the element geometry, FSSs can be classified into four categories of filter responses: band stop; band pass; low pass; and high pass filters, as shown in Figure 2.2. A perfect example of an FSS is the metal perforated door of a standard household microwave-oven. This FSS is similar to the high pass filter example shown in Figure 2.2, except the microwave-oven door has circular holes rather than square apertures. Acting as a high pass filter, the oven door blocks the 2.4GHz microwaves inside the oven but allows visible light (which is at a much higher frequency 400THz-700THz) to pass through, so the cooking progress can be monitored. In other words, although the oven door is optically `transparent', it essentially acts like a closed metal shield to the internal 2.4GHz microwave transmissions. The FSS examples shown in Figure 2.2(a) and (b) are known as *Babinet duals* [4, 5]. Physically, they are a complementary pair; and electromagnetically, the transmission properties of one structure correspond to the reflection properties of the other. Similarly, Figure 2.2(c) and (d) is another example of a pair of Babinet duals. In general, Figure 2.2(a) and (c) belong to the patch element family, whereas Figure 2.2(b) and (d) belong to the aperture or slot family. The element shape is not just limited to square loops or patches, as illustrated in Figure 2.3, the element can be circular rings, or tripoles, or more convoluted shapes.

The oldest reference to periodic surfaces dates back to 1919 in a patent granted to Marconi and Franklin for a parabolic reflector constructed from wire sections rather than long rods [2, pp5-9]. Studies of periodic structures (or FSSs) did not intensify until the 1960s, when their potential in military applications was realized | especially in stealth technology. Since the 1960s, FSSs have been widely used in the field of antenna design, radar and satellite communications. For example, FSSs are frequently used as sub-reflectors in the Cassegrain system with parabolic dish antennas, as illustrated in Figure 2.4(a) [2, p17]. Such reflectors are sometimes referred to as dichroic structures, which are transparent to one frequency band $f1$ but opaque to another frequency band $f2$. The dichroic structure creates two distinct focal points for placing two feed horns that operate at $f1$ and $f2$ respectively. As a result, the two frequency bands, $f1$ and $f2$, can be efficiently and economically accommodated by the same main reflector. Another example of FSS applications is in antenna radomes or for electromagnetic shielding, as illustrated in Figure 2.4(b) [2, p16]. Again, the FSS radome reflects unwanted transmissions in frequency band $f2$ while allowing desirable transmissions in frequency band $f1$ to pass through. Depending on the radome's shape, transmitted signals that are not in the operating band can be deliberately reflected away in certain directions to reduce the radar cross-section of an antenna [2, pp14-18]. Therefore, this radome application is widely deployed for military uses on missiles, aircraft or aboard ships

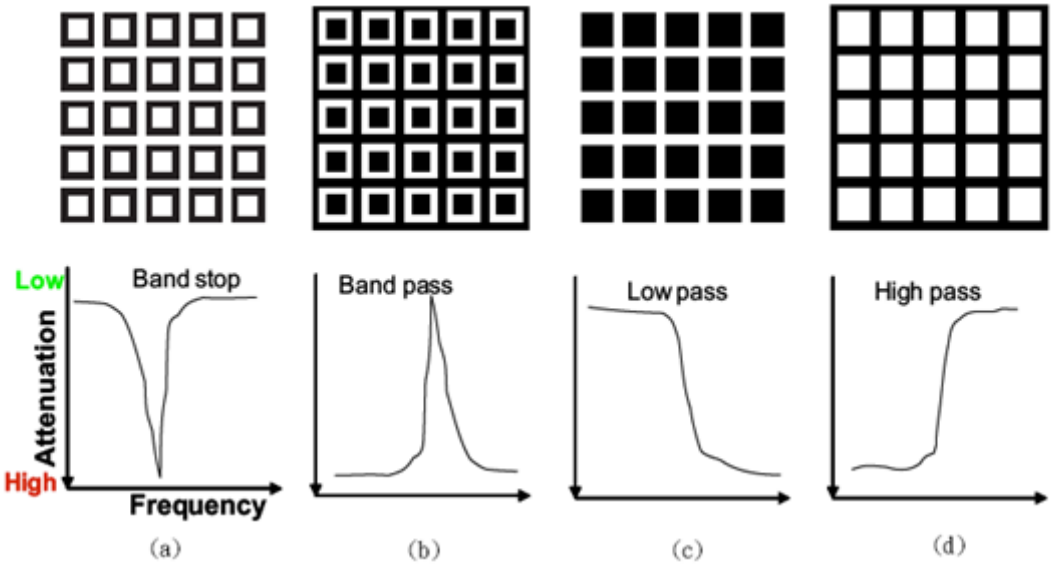

Figure: 2.2 Four basic FSS filters. Conducting materials are represented in black.

2.4 Complementary surfaces and babinet's principle

If placing the dipole array on top of the slot array leads to a complete ,infinite ,perfectly conducting surface, the two surfaces are called complementary to each other .In that case the reflection and transmission coefficients for one of them equal the transmission and reflection coefficients of the other, respectively .

This is a simple example of babinet's principle, which is well known from optics. For it to be valid, however we must observe certain requirement:

1. The surfaces must be perfectly conducting and "infinitely thin". In practice the screen thickness should be less than ~1/1000λ in order for babinet's principle to be reasonably accurate.

2. Adding a thin layer (< ~0.05λ)of dielectric will lead to a lower resonant frequency in both the dipole and the slot cases of approximately the same amount .however ,use of thicker slaps leads to quite different results for the two cases.

3. Cascading two or more surfaces behind each other leads to radically different transmission and reflection curves in the two cases.

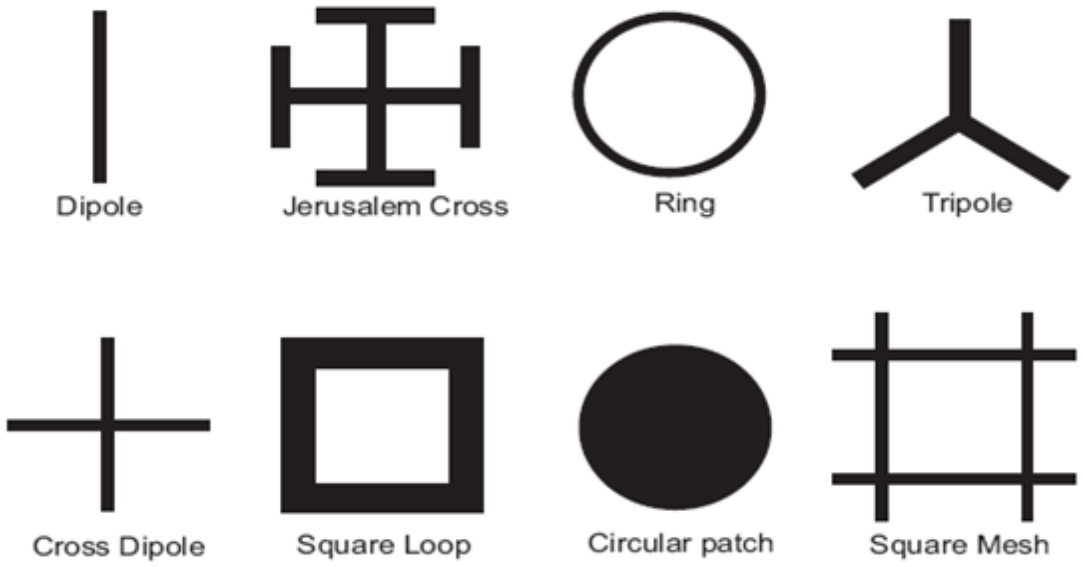

Figure: 2.3 Common FSS element shapes.

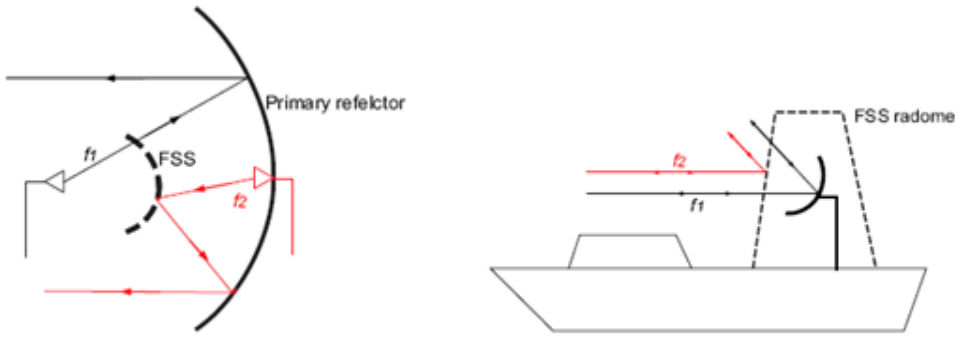

(a) A dual-frequency reflector antenna with an FSS sub-reflector.

(b) A hybrid antenna radome for military applications.

Figure: 2.4 Common FSS applications.

2.5 Factors which govern the FSS response

This section reviews factors which influence or govern the FSS response. Factors can be summarized into four main aspects, which are: the FSS's element geometry; the FSS's element conductivity; the dielectric substrate which supports the FSS; and the signal incident angles. The element geometry (including element shape) is a fundamental aspect a designer should determine in FSS design. Both the element conductivity and the dielectric substrate's permittivity have a great influence on FSS design and manufacturing, such as determining the materials required for making the FSS. In addition, the FSS performance at different signal incident angles is an important design criterion to consider. Because in reality, signals arrive on a wall at various angles, it is desirable to design an FSS that functions consistently over a wide range of incident angles.

2.5.1 Element geometry

The shape of the conducting element which constitutes an FSS is unrestricted. According to Munk [2, pp. 26-28], element shapes can be generally categorized into four basic groups, namely

1. Centre connected: such as dipoles, tri poles, Jerusalem crosses, and cross dipoles [10-12];

2. Loop types: such as square loops and rings [13-15];

3. Solid interior types: usually in the form of patches or apertures. For example, circular Patches and square meshes [16]; and

4. Combinations: sophisticated patterns with combinations of any of the centre connected, loop or solid interior shapes to overcome FSS performance deficiencies that are associated with simple element shapes [17-19].

Some common shapes are illustrated in Figure 2.3. Each shape possesses its own unique frequency characteristics. Some may be more sensitive to incident angles but allow a rapid transition between pass and stop bands. Other shapes may offer a desirable wide operating bandwidth, but perform inconsistently between vertical and horizontal signal polarizations. Table 2.1 [1, pp4-5] summarizes the performance of some common shapes relative to others, based on a single layer freestanding FSS. Table 2.1 shows that the square loop (SL) outperforms other types of element shape as it is rated 1 in every performance characteristic investigated. The SL element resonates and results in a bandstop response when each half-loop acts as a dipole element (i.e. when the length of each half-loop is a multiple of a half-wavelength). This bandstop response can be modeled by an equivalent LC circuit [14] illustrated in Figure 2.5. For a chosen element shape, such as the SL in this research, the general selective characteristic of an FSS is chosen to be bandstop; however the specific frequency response is determined by the element dimensions p*, d, g, s* as depicted in Figure 2.5. For instance, the separation

Element shapes	Angular stability	Cross polarization level	Larger bandwidth	Small band separation
Dipole	4	1	4	1
Jerusalem cross	2	3	2	2
Ring	1	2	1	1
Tripole	3	3	3	2
Cross dipole	3	3	3	3
Square loop	1	1	1	1

Table 2.1 Performance of FSS (1 is for the best performance and 4 is for worst)

period p, dimension d of the loop, and width of the conducting strip s, determine the location of the resonant frequency f_r, where the inter-element spacing (IES) g controls the FSS angular performance [14, 20]. Studies have suggested that a smaller square loop size generally results in a higher f_r, and a smaller g ensures stable f_r with varying incident angles [2, p8] [12, 21]. Research has shown that with more sophisticated element patterns (such as convoluted shapes [3, 21, 22], or by employing multiple layers of FSSs [3, 18, 23, 24]), better FSS frequency characteristics can be achieved. For example, a double-loop element as shown in Figure 3.6 can

offer multiple stopbands [15, 20], which is similar to cascading two FSSs with different SL dimensions, as described in [25]. It has also been suggested in [2, 18] that by cascading two slot FSSs in parallel, a broad passband can be obtained with a stable response to varying incident angles.

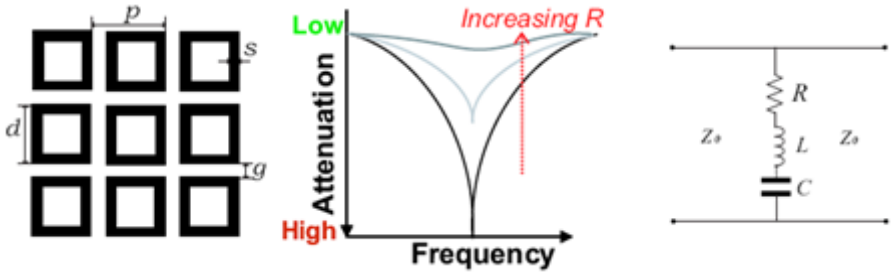

Figure: 2.5 the frequency response and the equivalent circuit model for the SL FSS, with varying element conductivities. *Z*0 is the characteristic impedance of the transmission line.

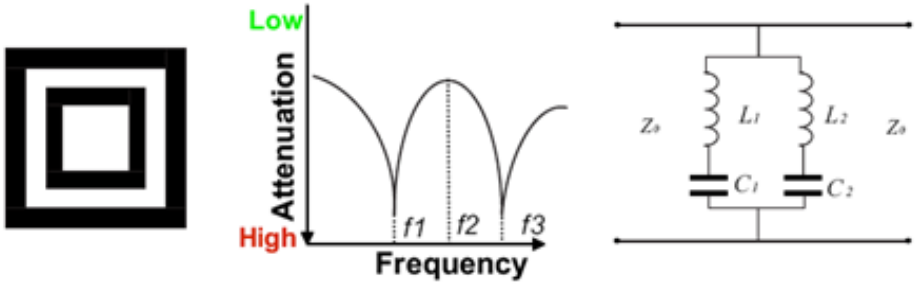

Figure: 2.6 The frequency response and the equivalent circuit model for the double square loop FSS *Z*0 is the characteristic impedance of the transmission line.

2.5.2 Element conductivity

Currents are induced on the conducting elements when electromagnetic (EM) energy is incident on an FSS. The induced current then reradiates EM waves from these conducting elements. Similar to conductive posts or strips inside a rectangular waveguide [26, pp280-285], the FSS can be modeled as energy-storing inductive or capacitive components in an equivalent circuit, which is determined by the element shape. For a lossy conductive material, power may be dissipated in the element. As a result, the overall FSS performance will be affected. For example, for a SL FSS, the low conductivity of the element can be represented by a resistor in series with the *L* and *C* component in the equivalent circuit, as illustrated in Figure 2.5. The introduction of a lossy component lessens the attenuation at the bandstop. In other words, the attenuation at the

resonant frequency *fr reduces* with increasing resistance until the FSS finally loses its frequency selective characteristics as shown in Figure 2.5 [3, p10].

2.5.3 Dielectric substrates

Dielectrics are often used to provide structural support or stabilizing the angular response of an FSS [10, 27]. For a single layer of FSS, arrangements of the FSS and dielectrics can be either (a) an FSS embedded or sandwiched centrally between dielectrics as shown in Figure 2.7(a); or (b) FSS attached to just one side of the dielectric substrate as shown in Figure 2.7(b). Due to the influence of surrounding dielectrics which change the FSS's equivalent capacitive component in the EC model, the resultant resonant frequency fr will be lowered by a factor of $\sqrt{\varepsilon_{eff}}$ from the *fr* originally designed. For a relatively thick dielectric substrate that is greater than 0.05 electrical wavelengths, the effective dielectric constant ε_{eff} equals the dielectric constant ε_r of the substrate for arrangement (a); and equals $(\varepsilon_r + 1)/2$ the arrangement (b). However, for a substrate with thickness less than 0.05 electrical wavelengths, the effective permittivity ε_{eff} is a nonlinear function of the substrate thickness [2, pp394-396]. In other words, the ε_{eff} becomes very sensitive to the substrate thickness. Accordingly, the *fr* will be sensitive to the substrate thickness. This may be because for a thin dielectric substrate, higher order evanescent modes that are excited by the conducting elements may still be significant at the air and dielectric boundary, which can modify the energy stored close to the FSS elements and hence change the resultant *fr* [10]. This suggests that the influence of a thin dielectric layer which holds the FSS elements in place cannot be neglected. Research has also indicated that above a certain frequency *fs*, higher order modes may propagate within the dielectric substrate, causing a series of complicated resonances. This phenomenon is sometimes explained as surface waves trapped in the dielectric substrate [10]. Such an *fs* is considered to be the upper limit of the operating frequency, and is associated with Wood's anomaly and occurrence of grating lobes [1]. Note that with the presence of a dielectric substrate, the *fs* for surface waves and the frequency where grating lobes begin to propagate do not alter substantially. The surface waves will not be eliminated if an FSS is embedded in dielectrics, but they can be pushed to a higher frequency if the dielectric is thin. Therefore, in order to achieve a wide operating frequency range with a significant separation between resonance *fr* and the upper limit *fs*, *fr* should be kept low and the *fs* high. This can be

done by (1) keeping the dielectric substrate thin, so that the *fs* remains at higher frequency (however this may be impractical for structural support); and (2) arranging dielectrics on both sides of an FSS rather than on just one side, so *fr* can be shifted downwards more, while *fs* remains unaffected in either case. Therefore, placing dielectrics on both sides of an FSS is usually the preferred arrangement [10].

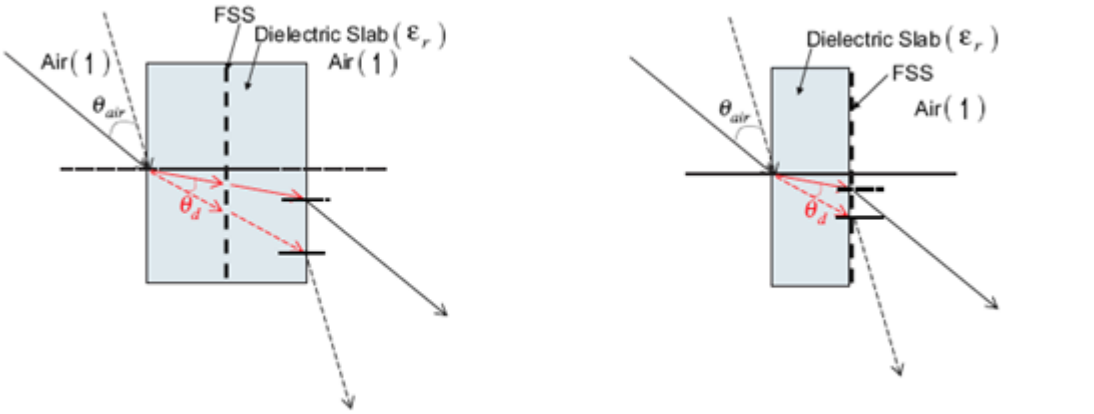

(a) FSS in dielectric substrates, $\varepsilon_{eff} = \varepsilon_r$. (b) FSS on a dielectric substrate, $\varepsilon_{eff} = (\varepsilon_r + 1)/2$.

Figure: 2.7 FSS in or on a thick dielectric substrate

Although different FSS/dielectric arrangements will influence the frequency selective response to a different extent, both arrangements improve the stability of FSS performance over a range of incident angles. In other words, with the use of dielectrics, FSS structures can be made less sensitive to incident angles. This is mainly because, according to Snell's law of refraction, the effective angle variation inside a dielectric layer is smaller than the actual angle variation in free space (i.e. $\mu_d < \mu_{air}$ as shown in Figure 2.7) [10]. Accordingly, the range of incident angle is reduced on the FSS elements inside the dielectric layer, making the FSS structure less angle sensitive.

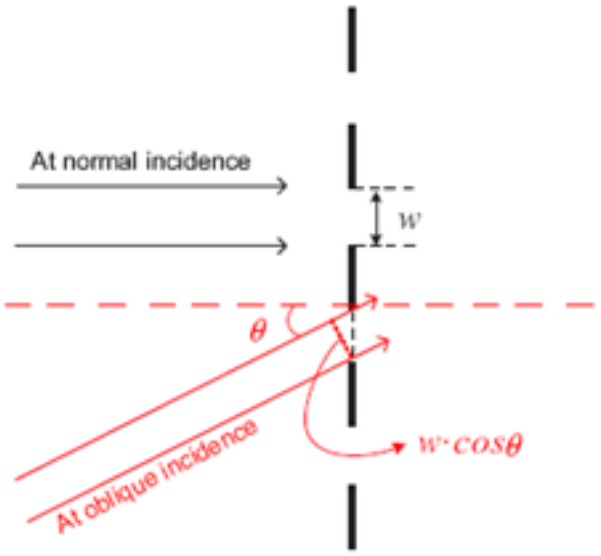

Figure: 2.8 Equivalent projected separation between elements by an obliquely incident signal.

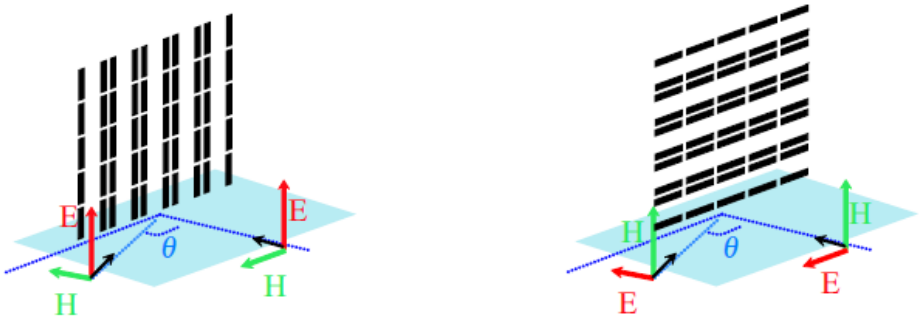

(a) The inductive component with TE-wave incidence (b) The inductive component with TM-wave incidence

Figure: 2.9 TE- and TM-wave incidence on inductive conducting strips, which the square loop elements are composed of.

2.5.4 Signal incident angles and polarizations

When a signal arrives at an oblique angle to an FSS with conducting strips periodically separated by *w*, as illustrated in Figure 2.8, the projected effective separation between each strip (and also the width of each strip) will be reduced by a factor of cosθ. The effective element dimensions seen by the oblique incident wave and accordingly the current induced differs from the scenario when the signal arrives at the FSS at 0°[13]. As a result, the FSS angular response varies [11, 20, 28-30].

This variation in FSS performance when the incident angle changes can also be demonstrated by the EC equations, These equations which calculate the equivalent inductive and capacitive value

of a SL FSS are a function of incident angle θ [26,31]. Therefore, the FSS resonant frequency is also a function of θ. For the SL FSS considered here, the resonant frequency will shift downwards with increasing θ [14, 32, and 33].

Apart from the varying incident angle, the polarization of the incident signal also influences the FSS response. For example, considering two vertical polarization scenarios TE-wave and TM-wave incidence as shown in Figure 2.9, though the E-field is polarized in the direction of conducting strips in both scenarios (so that strips can be modeled as an inductive component),currents induced on the strip are different when the incident angle becomes oblique. This is because in the TE-wave scenario, the E-field is always parallel to the strip and excites the full length of each strip regardless of incident angle; however, in the TM-wave scenario, the E-field arrives obliquely to the broadside of the strip, resulting in a shorter projected strip length as the incident angle increases.

2.6 FSS analysis techniques

Various techniques in analyzing scattering from periodic structures have been developed over the past four decades. This includes computational intensive approaches such as the method of moments (MoM) [42] or the mutual impedance method [2], the finite element method (FEM) [34], the finite-difference time-domain (FDTD) method [35, 36], and the simple analytical Equivalent Circuit (EC) method [14, 20]. Those techniques are briefly reviewed in this section without formulation details.

2.6.1 Method of Moments

The MoM is the most commonly used technique in analyzing scattering from an FSS. Many variations in analyzing FSSs using MoM have been developed [1, 37-40], but the earliest work reported in literature is the MoM approach presented by Chen [42]. Chen's approach is also sometimes referred as the modal (or integral equation) method. This method evaluates the current flows on the conducting elements by matching the tangential field at the surface of the element and forming an integral equation for the unknown current. More specifically, the unknown electric field, that is a function of unknown current, near the conducting element is expanded into a set of Floquet spatial harmonics; by satisfying the boundary conditions on the surface of the conducting element (i.e. the total electric field must be zero), an integral equation

for the unknown current is obtained. Then MoM is used to reduce the integral equation into a set of linear algebraic equations, which can be solved numerically.

2.6.2 FEM

An alternative approach for modeling the field scattered from a periodic structure is the finite element method (FEM) [34, 43-48]. FEM is a numerical procedure for obtaining solutions to boundary-value problems [49, p23]. The unknown field is discretised using a finite element mesh. Typically triangular elements are used for 2-D problems, and tetrahedrons are used for 3-D problems. The FEM may be derived via two different, but equivalent approaches `Ritz variational' or `Galerkin weighted' procedures. Both approaches start with the partial differential equation form of Maxwell's equations.

2.6.3 FDTD

As opposed to the MoM and FEM approaches which analyze the periodic structure in the frequency-domain, FDTD is a time-domain technique, so the solution can cover a wide frequency range in a single simulation run. The FDTD approach is a direct solution of Maxwell's time dependent curl equations [50, pp75-77]. The analysis is discretised in space and time, and equations are solved in a leap-frog manner to update the electromagnetic field within the computational domain considered (i.e. the electric field is solved at a given instant in time, then the magnetic field is solved at the next instant in time, and so on [51]). The computational domain will be gridded, and the E-field at a particular point on the grid will be updated depending on the previously stored H-field on both sides of the point. In a similar manner, the H-field can be updated. As a marching-on-in-time process, the E- and H-fields within and scattered from the structure can be determined [35, 36, 50, 52]. Additional examples of analyzing FSSs using the FDTD algorithm can be found in [53-55]. Because material properties can be specified at any given point in the computational domain, FDTD is capable of modeling arbitrarily shaped 3-D FSS structures with inhomogeneous dielectric substrates. However, the computational domain grids must be small compared to the wavelength, which may result in long solution time.

2.6.4 Mutual Impedance Methods

Munk [27] developed the mutual impedance method to evaluate the field scattered from an FSS. This method determines the voltage induced by the incident wave at the element and also the mutual impedance between elements. Current flows on the element can hence be verified. Built on the mutual impedance and plane wave expansion approach, Henderson [56] developed a periodic moment method (PMM) algorithm which can reliably model any arbitrarily shaped FSS elements or an FSS embedded in an arbitrary dielectric material. PMM has been employed in [2, 57, and 58] for FSS modeling or design.

2.6.5 Equivalent Circuit Models

In contrast to the above computationally intensive approaches, the EC model offers a simpler alternative method in FSS analyses. Based on a transmission line analogy, transmission characteristics of an FSS structure can be determined. The FSS is modeled as equivalent inductive and capacitive components in a transmission line, where the circuit components are evaluated based on the quasi-static EC approximation of conducting strips developed by Marcuvitz [4, 26]. Because it is a scalar technique, analysis is limited to linear polarizations and simple FSS element geometries. Although properties of dielectric substrates and signal incident angles can be taken into account in the EC equations, due to assumptions made in the EC approximation, the accuracy provided by the model may vary from case to case. Many studies have successfully employed the EC model in analyzing FSSs with simple element shapes such as square loops, meshes, linear dipoles, and Jerusalem crosses [11, 14, 15, 20, 29, 30, 41, 60]. Despite the less precise analysis offered by this EC approach compared to other methods, the EC model was chosen to be the preferred analyzing tool for this research. This is because the model provides results acceptably accurate for this research, and most importantly it can quickly characterize FSSs with varying element dimensions.

2.7 Summary of FSS analysis techniques

Numerical techniques such as the MoM, FEM and FDTD methods can be used to analyze complicated FSS structures. Especially both FEM and FDTD are capable of analyzing inhomogeneous substrates. However, to model an infinite periodic array, these techniques require considerable computer resources that are beyond the capacities of today's standard computers. Besides, these techniques only offer numerical approximations of the field. In

comparison, although the EC modeling technique is only recommended for dealing with simple FSS element shapes, it was chosen over other analyzing techniques in this research. This is primarily because the EC method requires little computer resource while still offering an acceptably accurate FSS analysis needed for indoor environments. Nonetheless, experimental measurements offer the most realistic and reliable examinations of FSS performance. Therefore, the analyses presented in this thesis have been based on EC modeling.

Chapter 3

FSS Design and Analysis by Equivalent Circuit Modeling

3.1 Introduction

In this chapter we will go through the analysis techniques of the FSS design. In the previous chapter we have discussed different analysis techniques but we have done the analysis through the equivalent circuit model because this modeling technique requires minimal computational resources, but provides reasonably accurate and fast predictions for FSSs with simple element shapes. Based on the equivalent inductive and capacitive components evaluated in the EC model, an FSS is represented by a 2×2 transmission matrix. The transmission matrix can easily integrate with matrices representing other materials to estimate the response of a multi-layered structure. This section presents the development of the EC model for SL FSSs.

3.2 Equivalent Circuit Models

The equivalent-circuit modeling technique was first applied to frequency-selective circuits by Anderson [61]. In the models the interaction of incident waves with an infinite periodic array of elements is represented as a wave travelling down a transmission line, with shunt lumped circuit impedances representing the array. For an infinite array of thin, continuous, perfectly conducting narrow strips the shunt impedance is either inductive or capacitive, depending on whether the incident wave is polarized parallel or perpendicular to the strips. In many practical arrays both inductive and capacitive components are present together, and their immittances vary at oblique angles according to whether TE- or TM incidence, or a combination of the two, occurs. Referring to Figure 3.1, for the inductive grating, TM-incidence occurs when the E-field is polarized parallel to the plane of incidence, i.e. $\theta = 0°$, and TE-incidence when the E-field is perpendicular to the plane of incidence, i.e. $\Phi = 0°$. Modeling arrays at oblique angles of incidence therefore requires expressions for the immittances for both TE- and TM incidence. Using the geometry of Figure 3.1, for conductors of periodicity *p,* width w and spaced a distance *g* apart, Marcuvitz gave normalized immittance expressions for two cases which will be described further.

3.3 The Single Square Loop Element

Among the different design we have chosen the square loop element because of uncomplicated modeling and superior performance in comparison with different designs in terms of angular response stability, the available operating bandwidth, and the cross-polarization level as shown in the table in previous chapter.

For SL elements, resonance occurs when each half loop acts as a dipole [62, p5] [63]. The design rule of thumb is hence to make the loop circumference approximately equal the resonant frequency's wavelength. However, the criterion for grating lobe suppression also needs to be considered. This means the period *p* for repeating elements, as illustrated in Figure 3.2, has to be less than the shortest wavelength considered in the operating band for 0° signal incidence. For larger incident angles, *p* should be kept less than one-half of the wavelengths. These are however just a rule of thumb for determining a starting value for designing an FSS. The final element dimensions (*p, d, g, s*) need to be fine-tuned to meet the desired frequency response.

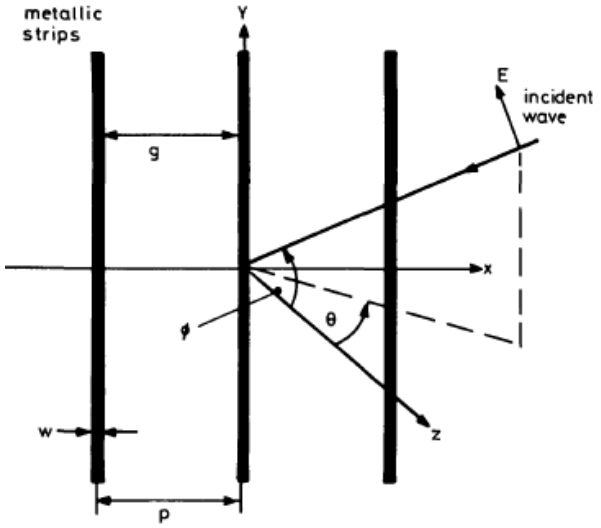

Figure: 3.1 *Plane wave incidents on an inductive strip grating* for a capacitive strip grating exchange the incident electric field E for a magnetic field H

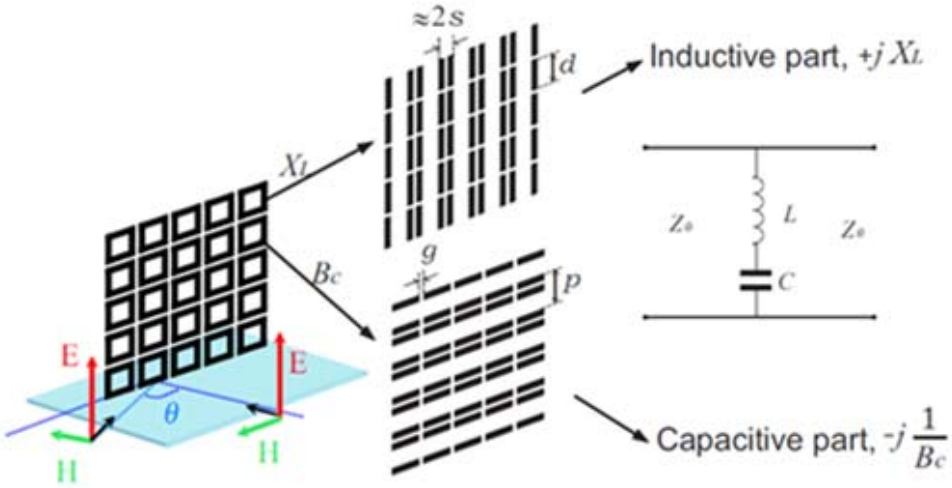

Figure: 3.2 The equivalent circuit approximation of square loop FSS with TE-wave incidence

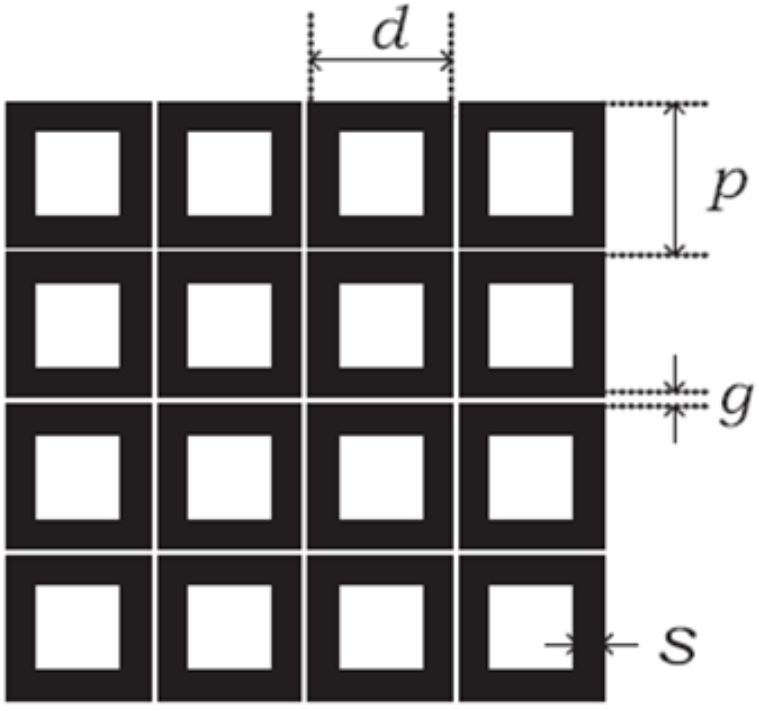

Figure: 3.3 The square loop element

3.4 The equivalent circuit development

An FSS layer can be represented by an equivalent circuit in a transmission line analogy as shown in Figure 3.2. The square loops are separated into vertical and horizontal conducting strips, which can be modeled respectively as inductive and capacitive components for TE-wave incidence.

3.5 Evaluation of the L and C components

For TE-wave incidence, as indicated in Figure 3.2, which has the electric field parallel to the vertical strips, the vertical strips can be modeled as a shunt inductive reactance in the EC circuit. The normalized impedance value *XL/Zo* is determined according to [64-65] as

$$\frac{X_L}{Z_o} = \frac{\omega L}{Z_o} = \frac{d}{p}\cos\theta\, F(p, 2s, \lambda, \theta) \tag{3.1}$$

$$F(p, w, \lambda, \theta) = \frac{p}{\lambda}\left[\ln \operatorname{cosec}\left(\frac{\pi w}{2p}\right) + G(p, w, \lambda, \theta)\right] \tag{3.2}$$

and

$$G(p, w, \lambda, \theta) = \frac{0.5(1-\beta^2)^2\left[\left(1-\frac{\beta^2}{4}\right)(A_+ + A_-) + 4\beta^2 A_+ A_-\right]}{\left(1-\frac{\beta^2}{4}\right) + \beta^2\left(1+\frac{\beta^2}{2}-\frac{\beta^4}{8}\right)(A_+ + A_-) + 2\beta^6 A_+ A_-} \tag{3.3}$$

With

$$A_\pm = \frac{1}{\sqrt{\left[1 \pm \frac{2p\sin\theta}{\lambda} - \left(\frac{p\cos\theta}{\lambda}\right)^2\right]}} - 1 \tag{3.4}$$

and $\beta = \sin\left(\frac{\pi w}{2p}\right)$

where λ is the wavelength in air at the operating frequency, θ is the incident angle at the FSS, and *w* is equal to 2*s* in this calculation.

Similarly, the horizontal strips which are parallel to the magnetic field (at 0° incidence) can be modeled as a shunt capacitive susceptance *Bc/Yo* according to

$$\frac{B_c}{Y_0} = \frac{\omega c}{Y_0} = 4\frac{d}{p}\sec\theta\, F(p, g, \lambda, \theta)\,\varepsilon_{eff} \tag{3.5}$$

Where ε_{eff} is the effective permittivity of the surrounding dielectric substrate that influences the capacitance value and *w* is equal to *g* in this case.

Equation (3.5) is crucial for modeling the FSS angular response accurately. This equation was developed from the general expression derived by Archer [66], which accounts for the capacitive component yielded from TE-wave incidence at oblique angles. Equations (3.1)-(3.5) are all built on the EC model developed by Marcuvitz [67, pp280-284], which approximates the effect of conducting strips in a waveguide structure. Here, because the conducting strips are segmented into a series of finite strips, a factor of *d=p* was introduced in both (3.1) and (3.5) to account for the effect of discontinuous strips.

Equations presented here have shown that the FSS response is a function of SL element dimensions, operating frequencies, incident angles, and the dielectric material next to the FSS. It is worth noting that for modeling the vertical strips to obtain the equivalent inductive impedance, two adjacent strips are approximated as one strip with width equal to 2*s* [63]. The validity of this assumption is weakened if the gap *g* between each element is large. Therefore, different prediction accuracies may be expected from the EC model for modeling FSSs with elements that are sparsely-packed or densely-packed. Note that the equivalent circuit equations presented here are valid for $p\ (1 + \sin\Theta) < \lambda$, only, which is the same as the criterion for suppressing the grating lobe as explained in the previous chapter. When this criterion is violated, $A_{\mp}$ in (Equation 3.4) becomes complex, resulting in a real part in *jXL* and *jBc*. This implies that the SL element can no longer be modeled as pure inductive or capacitive components which store energy. The real part suggests power dissipation due to the occurrence of grating lobes.

3.6 Double Square FSS and Their Equivalent Circuit Model

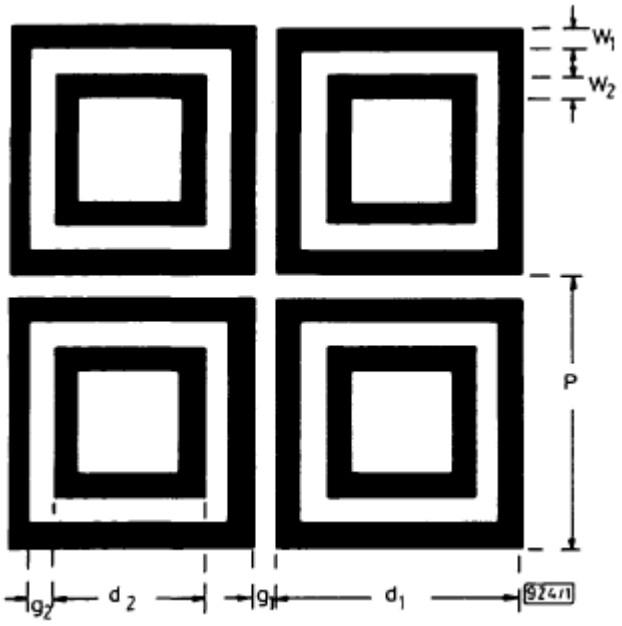

Figure: 3.4 Geometry of square loop array

Array elements having a double resonant-frequency transmission characteristic can be used as single-layer frequency selective surfaces. These types of arrays have two resonant frequencies. The first resonant frequency *f1* is independent of the inner square side *d2* but dependent on its width w2. The second resonant frequency *f2* is determined by the inner-square dimensions only,*f*2 increasing as *d2* decreases.

Figure 3.5 shows the equivalent circuit for the double square loop array. The basic equations for calculating the inductance and capacitance of strip gratings are found in Marcuvitz, and in general form are given by the equation (3.1-3.5).

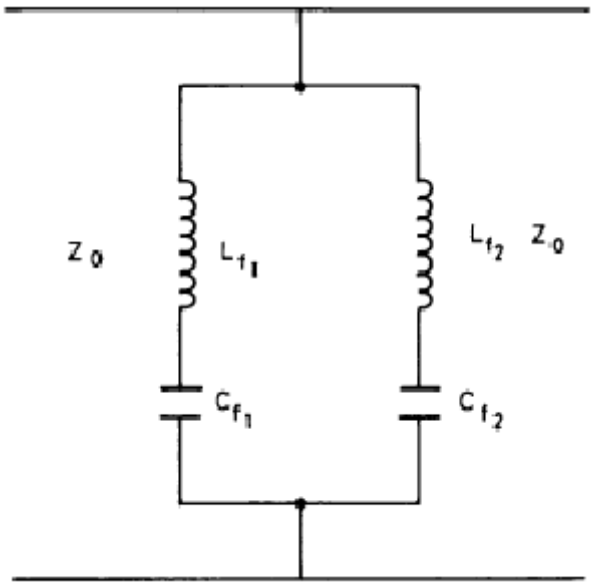

Figure: 3.5 Equivalent circuit for double square loop

The four circuit elements given in Figure 4.4, L_{f1}, C_{f1}, L_{f2}, and C_{f2} are calculated as:

$$L_{f1} = 2.0 * \left(L_1/L_2\right) * \frac{d_1}{p} \qquad where\ L_1 - F(p, w_1, \lambda)\ and\ L_2 - F(p, w_2, \lambda)$$

$$C_{f1} = 0.75 * C_1 * \frac{d_1}{p} \qquad where\ C_1 = 4F(p, g_1, \lambda)$$

$$L_{f2} = L_3 * \frac{d_2}{p} \qquad where\ L_3 = F(p, 2w_2, \lambda)$$

$$C_{f2} = (C_1\ in\ series\ with\ C_2) \qquad where\ C_2 = 4F(p, g_2, \lambda)$$

3.7 Simulated Results:

1. Double square loop with a patch type element

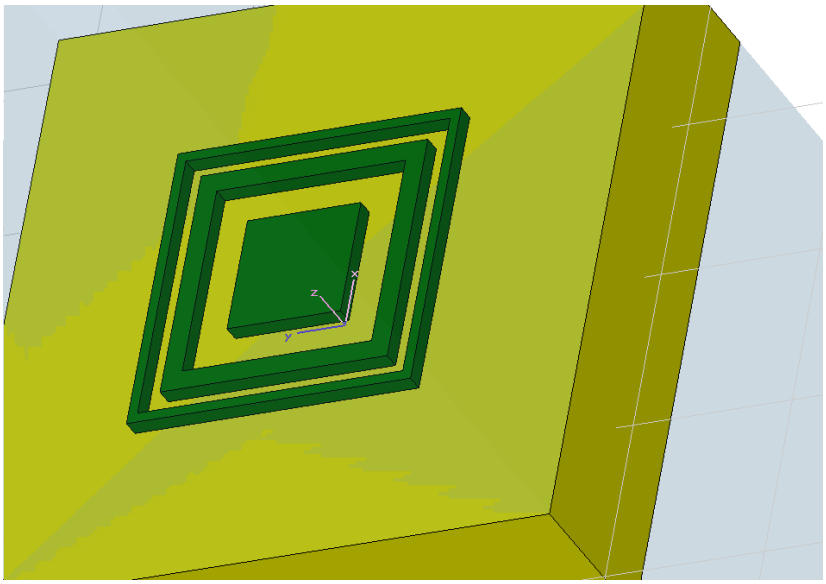

Figure: 3.6 Double square loop with a patch type element

Superstrate is made up of copper with the thickness of 0.1mm. Substrate is made up of the material with relative permittivity 6.15 and loss tangent 0.0025 and the thickness of the substrate is 1.016mm. length and breadth is 3.8mm.

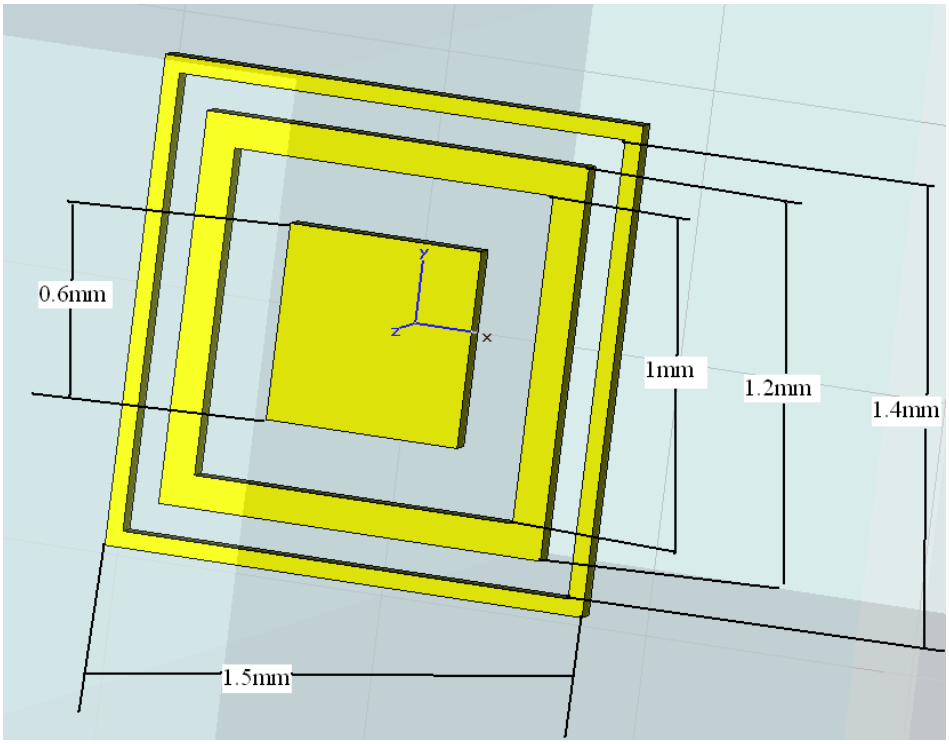

Figure: 3.7 Dimensions of double square loop with a patch type element

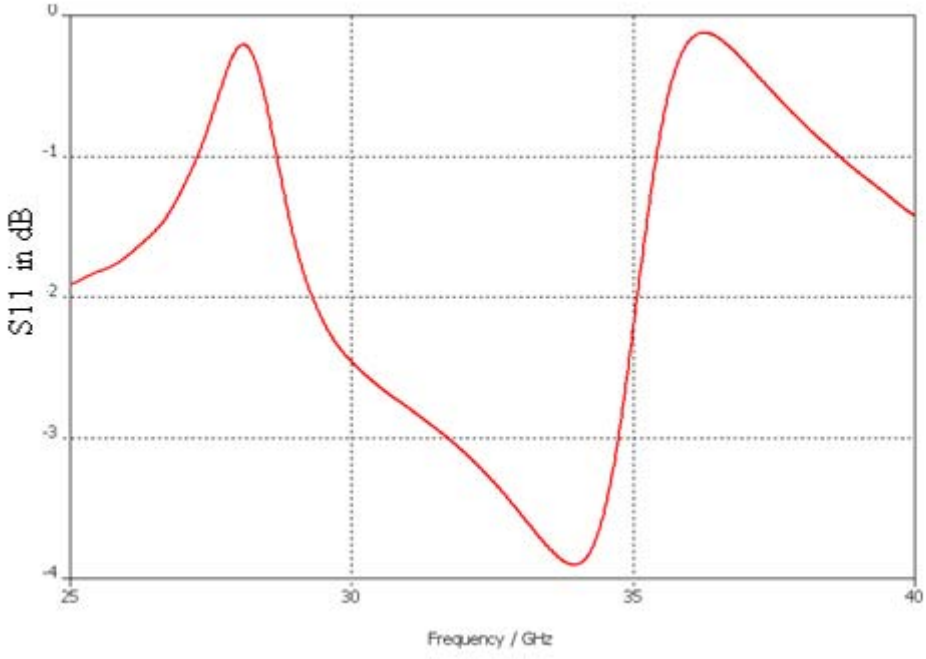

Figure: 3.8 Transmission coefficient of double square loop

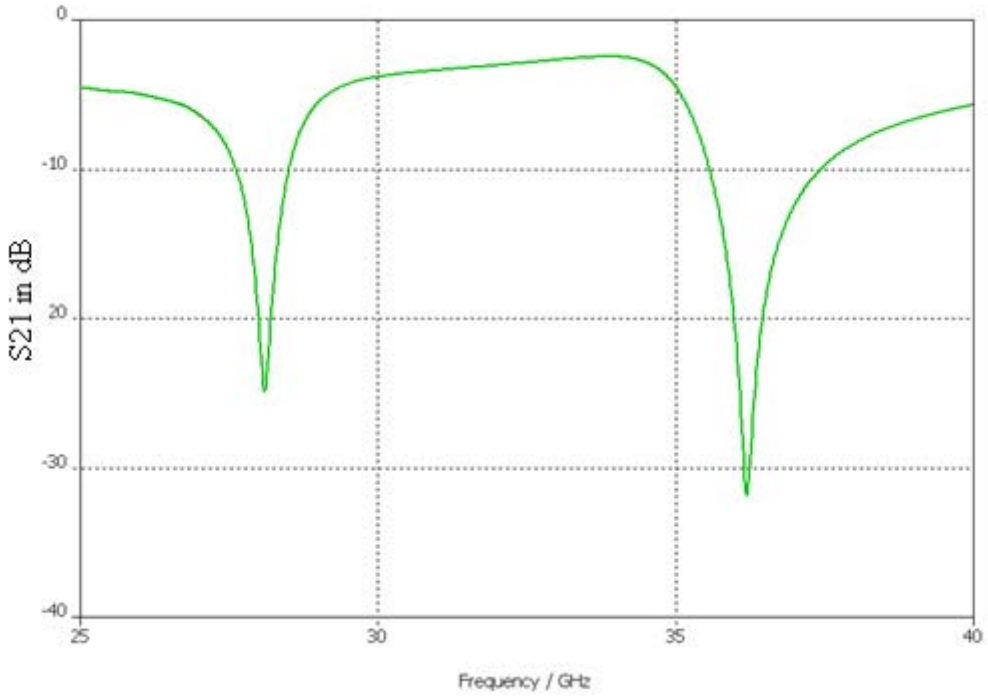

Figure: 3.9 Reflection coefficient of double square loop

2. Center connected element (Jerusalem cross element) :

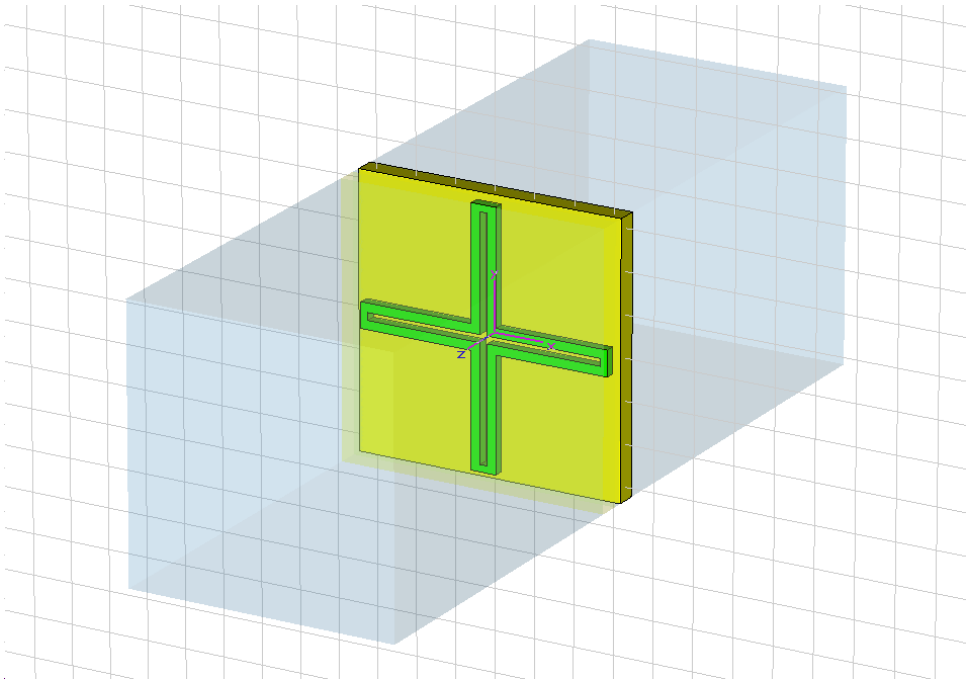

Figure: 3.10 Center connected element

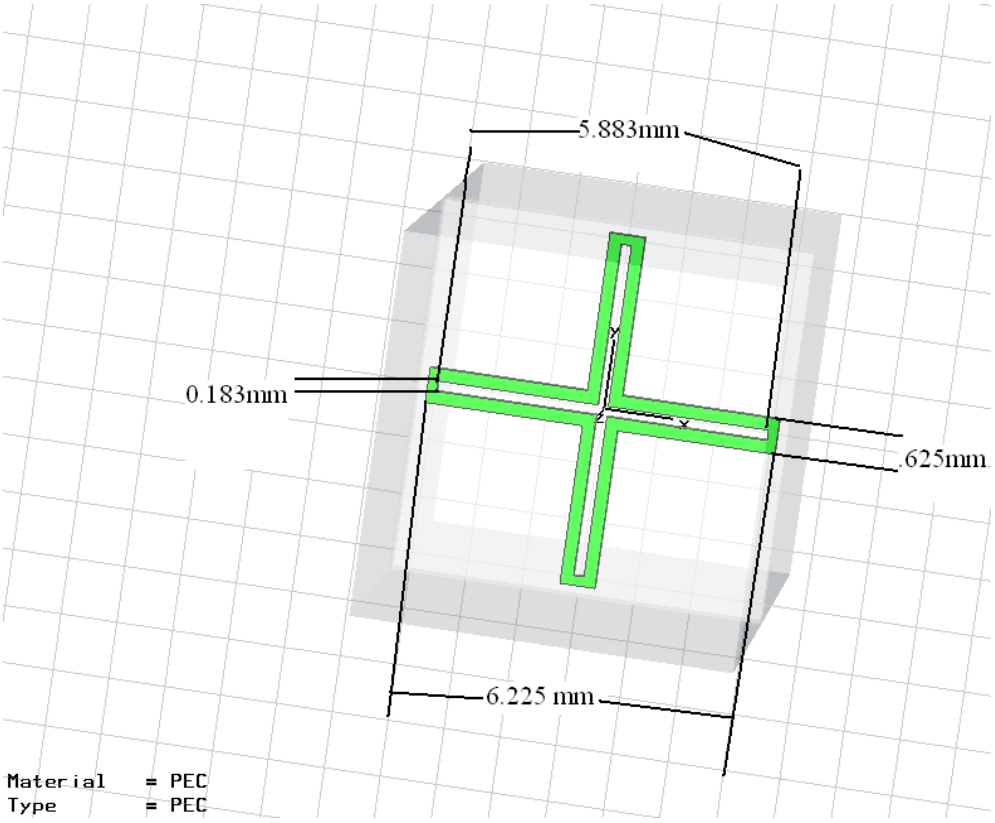

Figure:3.11 Dimensions center connected element

Relative permittivity of substrate is 2.2 Material of superstrate is PEC

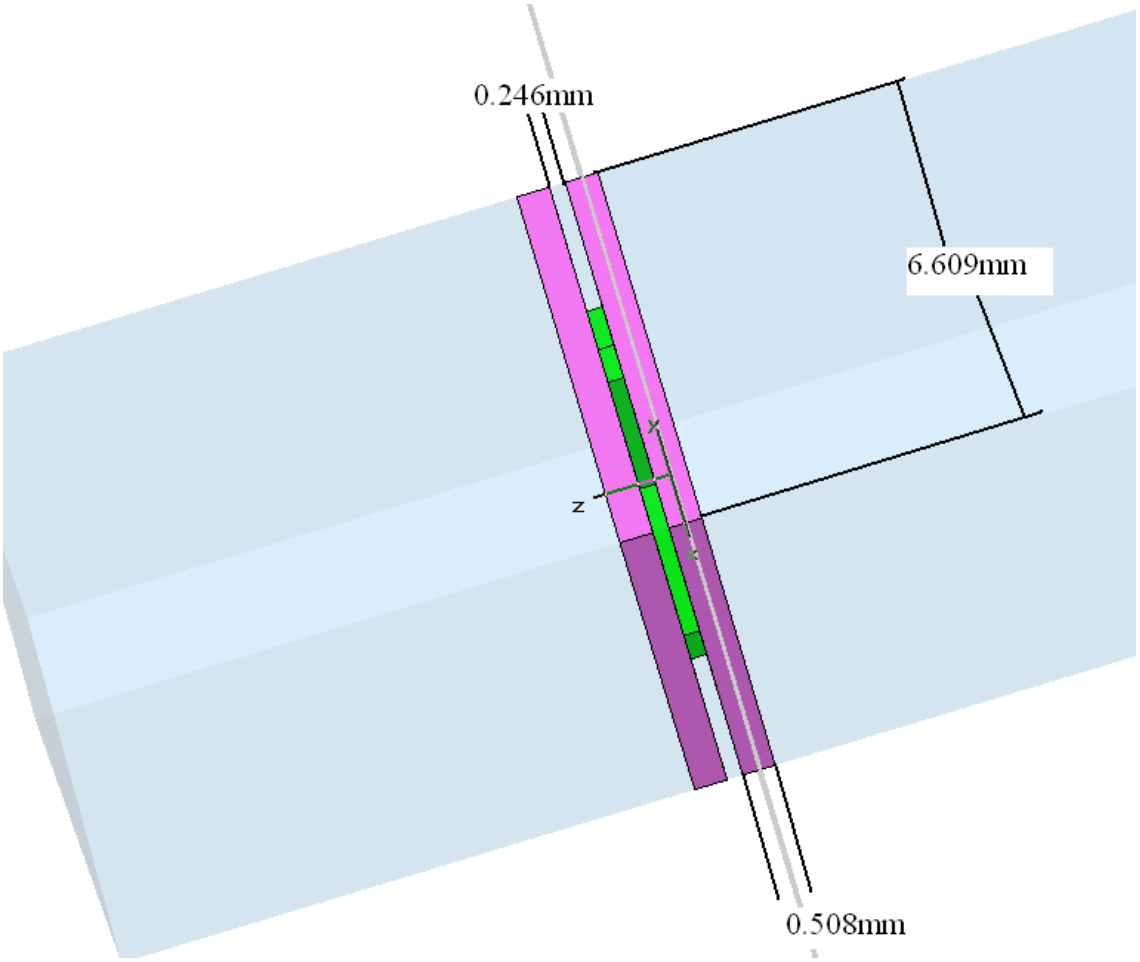

Figure: 3.12 Dimensions Center connected element

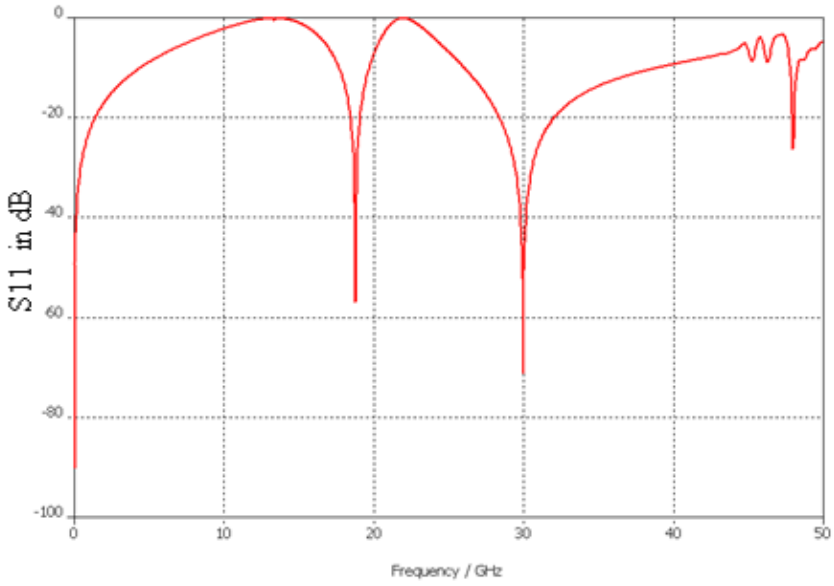

Figure: 3.13 transmission coefficient of centre connected

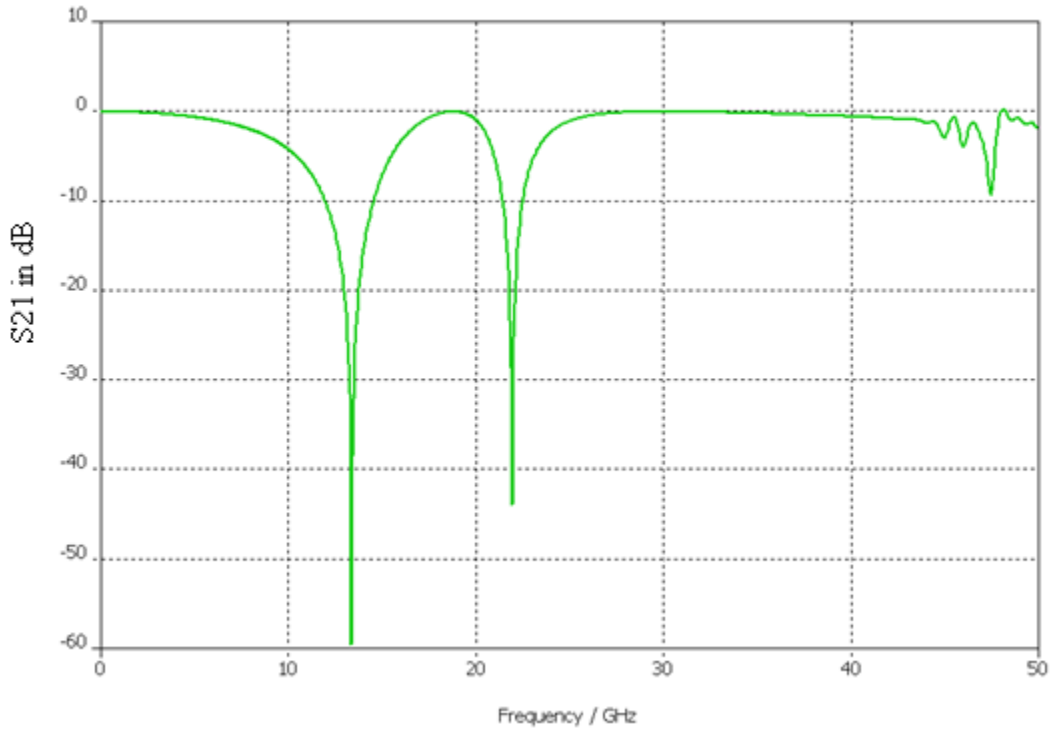

Figure: 3.14 Reflection coefficient of centre connected

3. Single square loop element:

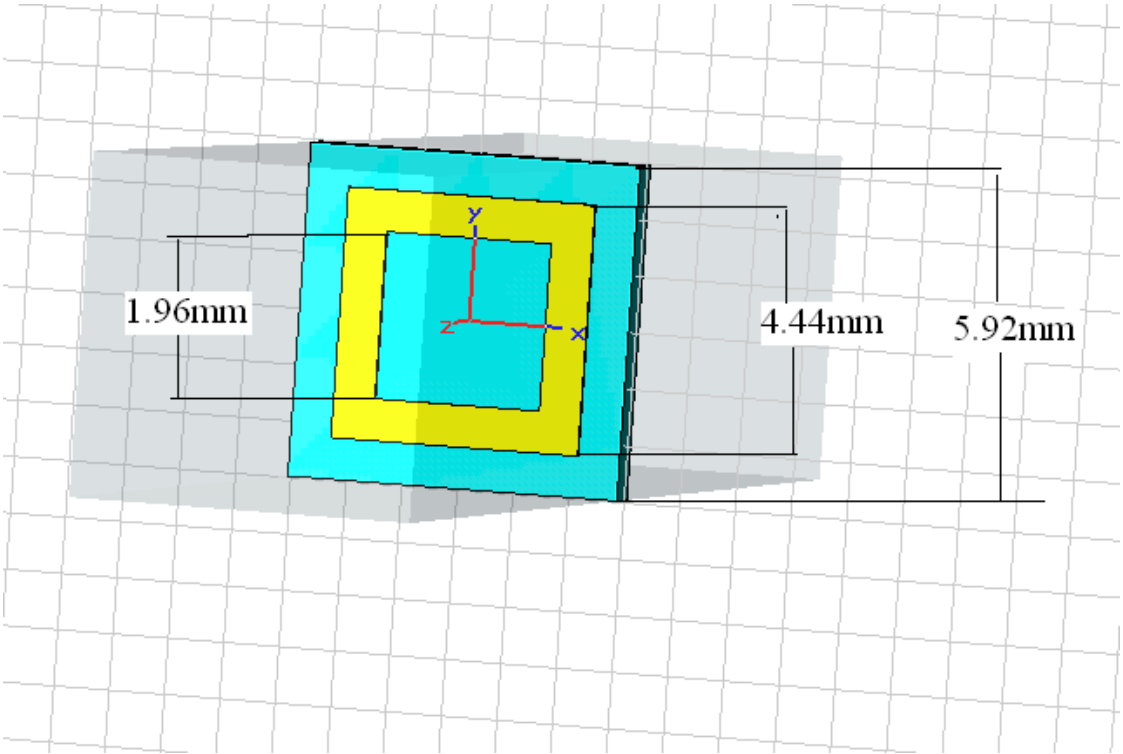

Figure: 3.15 Single square loop element

Superstrate is made up of aluminum with the thickness of 0.08mm. substrate is made up of normal material with thickness of 1.0mm and relative permittivity is 1.

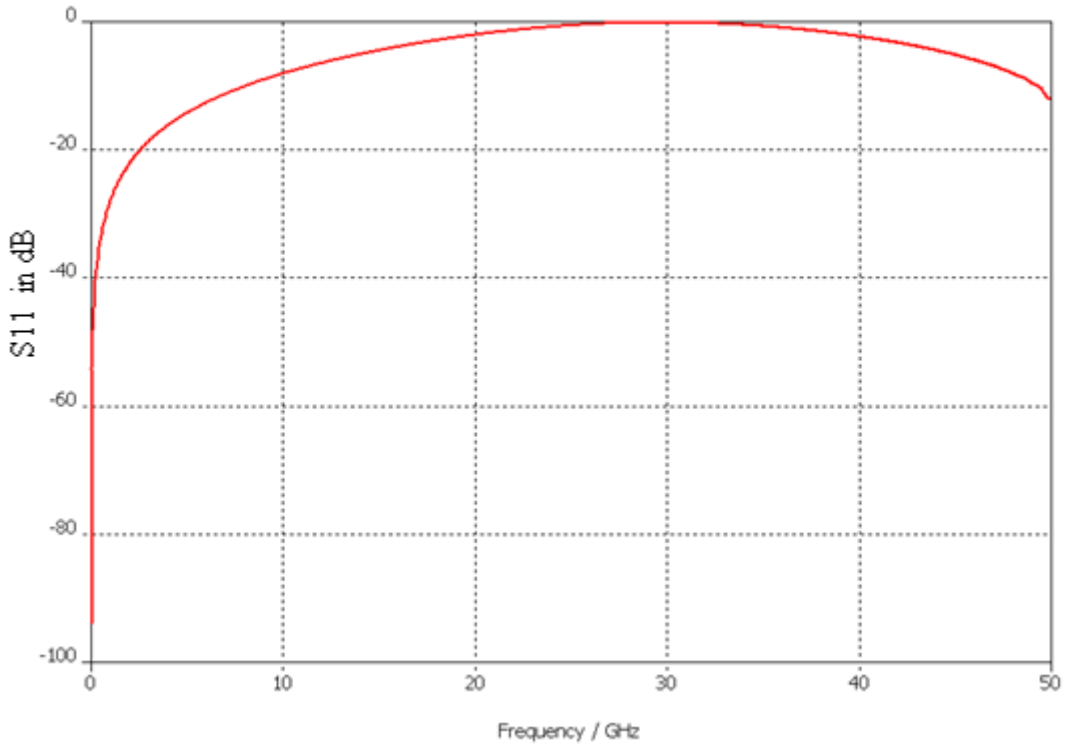

Figure: 3.16 Transmission coefficient of single square loop

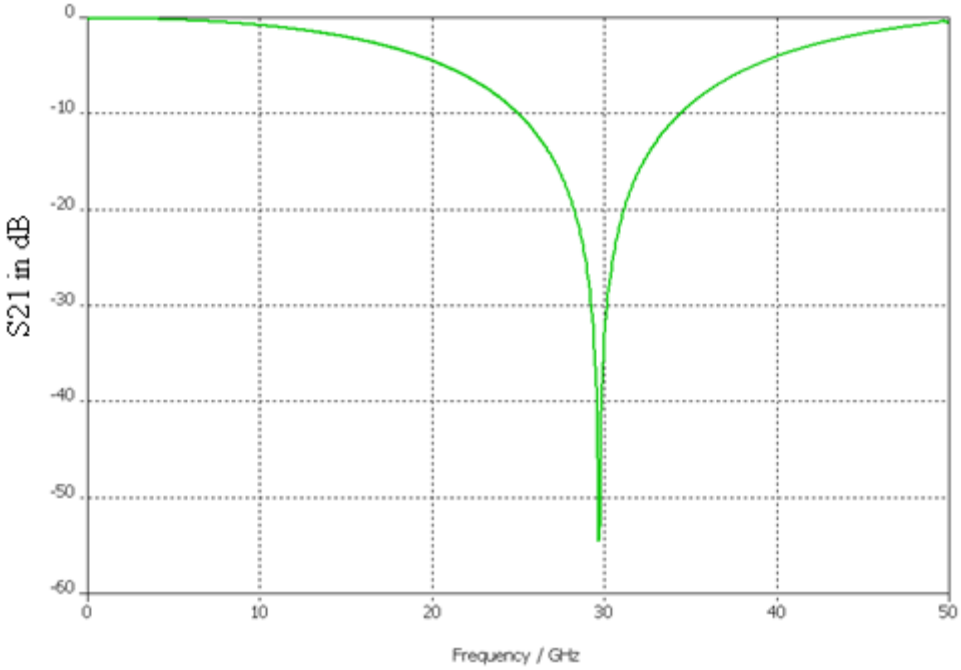

Figure: 3.17 Reflection coefficient of single square loop

Chapter 4

Dielectric rod antenna

4.1 Introduction

Recently, with the explosive growth of wireless communication, antennas become undoubtedly an essential part of the telecommunication system and the demand on the antenna development has driven designers to device a variety of antennas. The dielectric rod antennas are of considerable interest as high gain antenna for high throughput communication at microwave and millimeter wave frequencies. They are commonly based on the concept of surface wave discontinuity. Moreover, the dielectric rod antenna is a good Gaussian beam launcher.
Dielectric resonator antennas and dielectric rod waveguide antennas are good alternatives for millimeter wave lengths due to low losses and radiation. Dielectric rod waveguide antennas also have lot of advantages, they offer wide operating frequency band, their rectangular form has good integrability, lower losses, wider tolerance, low cost than standard metal wave guides in millimeter wave range and light weight. The dielectric rod wave guide antenna can be designed to have radiation patterns that change only little over a large frequency band. They can have a flat region in radiation pattern around the bore sight. [69, 70]

The dielectric rod antenna belongs to the family of surface wave antennas. The radiation mechanism of dielectric rod antenna can be explained by the discontinuity radiation concept [71] in which the antenna is regarded as an array composed of two effective sources at the feed end and free end of the rod. Part of the power excited at the feed end is converted into guided wave power and is transformed into radiation power at the free end. The remaining power is converted into unguided wave power radiating near the feed end. Therefore the directivity of the dielectric rod antenna is characterized by the directivities generated by the two effective sources [72]. In general, the dielectric rod antenna is linear or curvilinear tapered [73, 74]. Here we have proposed a design of linearly tapered antenna.

In this project, we have simulated a dual-band dielectric rod antenna at 29GHz and 32.6GHz frequency for advanced communication systems. Here we emphasize to demonstrate the discontinuity radiation concept for a dielectric rod antenna fed by a metallic waveguide with a

planer ground plane and to show how the use of discontinuity radiation concept enhances the computational efficiency of the design of large dielectric rod antenna.

4.2 Traveling-wave antenna

Traveling-wave antennas consist of transmission-line structures that radiate. To first order, length determines gain and bandwidth. The size and shape of the structure produce secondary effects such as polarization nulls and narrower beam widths. Most of these structures are slow wave-transmission structures that bind waves to it and radiate at discontinuities. We use surface-wave structures to radiate end-fire beams and leaky wave structures to radiate beams at an angle to the axis of the line source. One can make travelling-wave antennas from structures that guide waves. Surface-wave structures bind the power to the transmission line and radiate from discontinuities such as bends or dimensional changes.

There are mainly two types of travelling wave antenna:

4.2.1. Slow wave (surface wave)

A slow wave exists on an open transmission-line structure that binds the wave by slowing a passing wave and bending it in the direction of the structure. In the same manner, a lens bends waves toward regions of higher index of refraction. We designate x as the direction normal to a planar structure and the radial Coordinate ρ as the direction normal to the cylindrical slow-wave structure. The relation between propagation constants in various directions is

$$k_z^2 + k_x^2 = k^2$$

Since x (or ρ) is unbounded, the waves must attenuate exponentially from the surface:

$$\alpha = jk_x \qquad (4.1)$$

The z-directed propagation constant becomes

$$p = \sqrt{1 + \frac{\alpha^2}{k^2}} = \sqrt{1 + \left(\frac{\lambda\alpha}{2\pi}\right)^2}$$

4.2.2. Fast Waves (Leaky Wave Structure)

Only closed structures such as waveguides support fast waves. An open structure requires a negative α (eqn4 .1) for fast waves, which implies an exponentially increasing wave away from the structure. The structure soon radiates all its power and no longer guides the wave.
The waveguide propagation constant determines the direction of radiation from a travelling wave leaking out of the guide at a slow rate.

4.2.3 Radiation of surface-wave Antennas

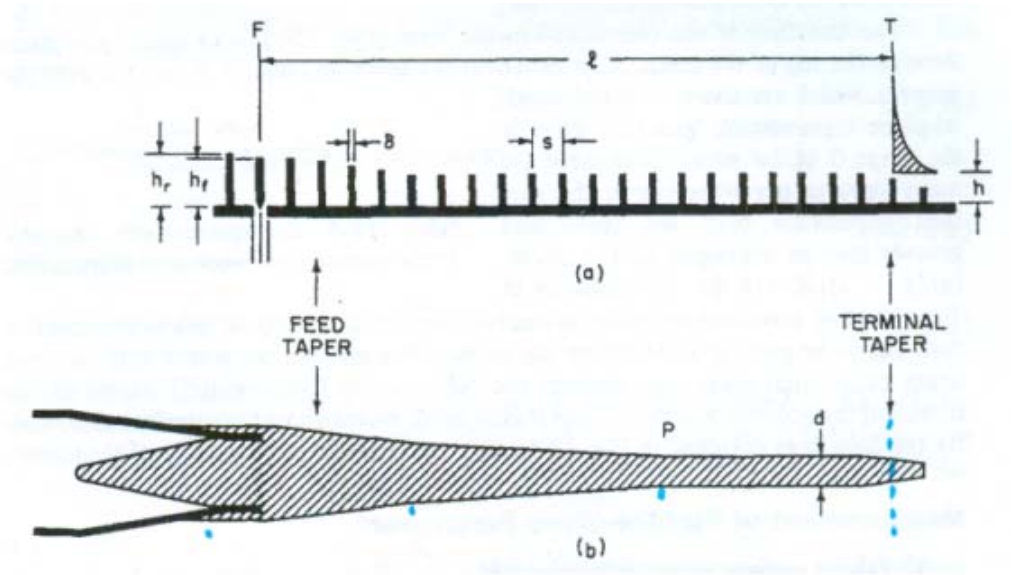

Figure: 4.1 surface wave antenna (a) yagi uda antenna (b) dielectric rod antenna

Two typical structures of the surface wave antennas are shown in the above figure. The feed F (consisting of a monopole and reflector in Figure 4.1a and of a circular or rectangular waveguide in Figure 4.1b) couples a portion of input power into a surface wave, which travels along the antenna structure to the termination T, where it radiates into space. The ratio of power in surface wave to total input power is usually between 65 and 75 percent. Power not coupled into the surface wave is directly radiated by the feed when no antenna structure is in front of it.

The tapered regions in Figure 4.1 serve many purposes. The feed taper increases the efficiency of excitation and also affects the shape of the feed pattern. The body taper (extending to point P in Figure 4.1b) suppresses side lobes and increases bandwidth. Because a reflected surface wave spoils the pattern and bandwidth of the antenna, a terminal taper is employed to reduce the reflected surface wave to a negligible value.

4.3 Dielectric rod antenna

The dielectric rod antenna has a dielectrically filled circular waveguide section that serves as a feed for the dielectric rod. This is followed by a feed taper section that is mainly used for matching the feed to the dielectric rod. The main body of the antenna follows the feed taper and ends in a terminal taper as shown in Figure 4.2

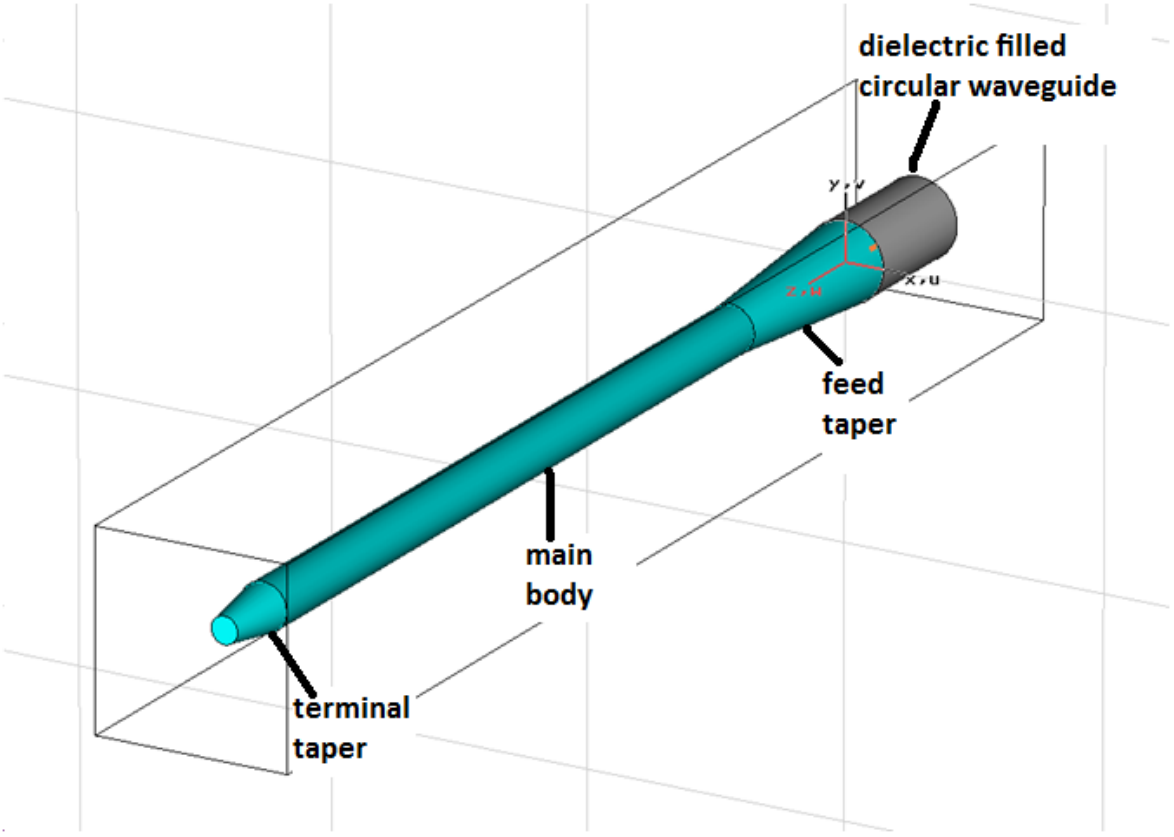

Figure 4.2: Dielectric rod antenna designed in CST.

The design of the stand alone antenna involves the lengths and diameters of the various sections in Figure. As explained in [76], the phenomena that govern the operation of the antenna can be

defined as two types of propagating waves. The antenna is fed by the dominant TE_{11} circular waveguide mode in the dielectrically filled section. At the feed edge discontinuity, where the metal circular waveguide ends, a hybrid mode surface wave HE_{11} is generated that is mostly contained by and propagates along the dielectric rod. The second propagating wave generated at the feed edge discontinuity is a radiated wave propagating through free space. The main body section of the rod is designed to support the HE_{11} mode, with the two taper sections serving to match the main body section to the feed and also to the free space radiation termination of the HE_{11} mode at the end of the rod. The lengths of the various sections are chosen to maximize the matching effects of the structure and to have the two propagating waves in phase at the termination of the rod.

4.4 Design principle of dielectric rod antenna

4.4.1 Diameter of rod

According to [76], fundamental single mode HE_{11} operation for the dielectric rod is guaranteed if:

$$\frac{d}{\lambda_0} = \frac{0.626}{\sqrt{\epsilon_r}}$$

d - The diameter of the rod

λ_0- The free space wavelength at the frequency of operation

ϵ_r - The dielectric constant of the rod material

This sets an upper limit to the diameter of the main body of the dielectric rod. Adherence to this guideline at the highest frequency of operation ensures single mode operation for the entire operational band. A lower limit to the diameter of the rod is that for which the HE_{11} containment in the rod becomes negligible. Smaller diameters, for which a breakdown in mode containment occurs, result in failure of assumed hybrid surface wave operation. Greater containment of the propagating energy within and around the dielectric rod is achieved for higher frequencies, given

the same dielectric rod dimensions. Consequently the breakdown diameter for the lowest frequency of operation determines the lower limit of rod diameter. Using these two limits the diameter of the main body section can be chosen. Manufacturing instructions should be such that any errors will add to the rod diameter rather than subtract, since propagation of some higher order mode components will be less of a problem than operational breakdown. In order to allow for useful band separation the dielectric constant of the rod should be at least 2, but it should not be so high that excessive modal disturbance of the TE_{11} Ka-band mode occurs [76]. In addition the commercial availability of mechanically compatible materials limits the scope of choice. A PTFE (Polytetrafluoroethylene) dielectric material with a dielectric constant of 2.55 was chosen for the design. This results in an upper radius limit of 1.96 mm, and a lower radius limit of 1.2 mm for the rod. A nominal design radius of 1.8 mm was consequently chosen, leaving ample manufacturing tolerance (> 6x 0.001") on the upper end of the range.

4.4.2 Length of antenna

As explained in [76], a minimum dielectric rod length is required for the hybrid surface wave to be well established. This length is stated as being where the phase of the radiated wave in the air leads the phase of the surface wave in the rod by 120 degree. As a result this length can be defined as

$$l_{min}k_z - l_{min}k_0 = \frac{\pi}{3}$$

l_{min} - The minimum required length in meters

k_0- The free space propagation constant

k_z - The propagation constant of the hybrid surface wave in the axial direction of the dielectric rod

The propagation constant of the HE_{11} mode in the axial direction of the rod plays a central role in the design of the rod antenna. The design of the rod antenna has to be performed at the highest operating frequency in the band, since the radiation performance of the antenna starts to deteriorate rapidly above the design frequency. At 30 GHz the HE_{11} mode propagation constant for a rod of 1.8 mm in diameter was calculated to be 655.96radians/meter. Extending the rod beyond the required minimum length serves the purpose of bringing the surface wave and the radiated wave into phase. The exact phase relation required for maximum antenna gain depends on a number of factors such as feed efficiency in exciting the HE_{11} mode, feed taper dimensions

and overall rod length. As a result the design choices for the total rod length are empirical in nature. A design equation is given in [7]:

$$\frac{\lambda_0}{\lambda_z} = 1 + \frac{\lambda_0}{pl}$$

λ_0 the free space wavelength

λ_z - the surface wave wavelength in the dielectric rod

p - an empirical optimization factor

l - the total length of the rod antenna

For antennas with expected lengths of between three to eight free space wavelengths, the suggested value for p is 3. Using the calculated propagation constant of the HE_{11}, mode in this equation yields a total rod antenna length of 76.982 mm. With the main body diameter and total antenna length calculated, all that remains is the design of the feed and terminal tapers.

If the efficiency of excitation were 100%, there would be no radiation from the feed. Consequently, there would be no interference with the terminal radiation and the antenna needs to be just long enough so that the surface wave is fully established; that is $l=l_{min}$.

$$l_{min}k_z - l_{min}k_0 = \frac{\pi}{3}$$

$$\Rightarrow \quad \frac{\lambda_0}{\lambda_z} = 1 + \frac{\lambda_0}{6l}$$

According to [76] the feed taper should be 0.2 times the total antenna length, yielding a value of 15.396 mm. The start diameter of the feed taper at the feed edge should be such that the ratio $\frac{\lambda_0}{\lambda_z}$ is between 1.2 and 1.3. To determine the correct diameter that would attain a value in this range, the propagation constant of the HE_{11} mode in the rod for various diameters were calculated, using below equation:

$$\frac{\lambda_0}{\lambda_z} = \frac{\beta}{k_0}$$

$\beta = k_z$ the propagation constant of the hybrid surface wave in the axial direction of the dielectric rod.

A diameter of 6 mm was chosen, yielding a ratio as defined above of 1.27. The fundamental mode in circular waveguide is the TE_{11} mode with a cutoff frequency as defined by the well known analytical expression [16]

$$f_{cutoff} = \frac{1.841}{2\pi\sqrt{\mu\epsilon}}$$

$$\mu = \mu_0\mu_r$$

$$\epsilon = \epsilon_0\epsilon_r$$

Using this expression the cutoff frequency for a circular metal waveguide filled with the chosen dielectric, having a diameter of 6 mm, is 18.336 GHz. The choice of a diameter of 6 mm for the start of the feed taper is therefore acceptable, since the Ku-band will be in cutoff but the Ka-band will be able to propagate. The next possible higher order mode in the circular waveguide is the TM_{11}mode. Since the circular waveguide is excited by the TE_{11} mode in the WR28 rectangular waveguide, the TE_{01} and TE_{01} modes in the circular waveguide will not be excited because of the incompatible modal field distributions. The cutoff frequency for the TM_{11} circular waveguide mode in the designed dielectrically filled circular waveguide is 38.166 GHz. The diameter of the dielectric rod at the end of the terminal taper should be such that the energy in the HE_{11} mode is no longer contained and radiation of the energy will occur. The best containment of energy in the rod is at the highest frequency. Consequently, this diameter should be designed at the highest frequency in the band, to ensure that containment is ended. At this diameter the propagation constant of the surface wave is approximately equal to the free space propagation constant ($\beta = k_0$), indicating a slow wave operational limit.

The diameter where containment starts to break down at 30 GHz is 2.4 mm. A diameter of 2 mm for the end of the terminal taper was consequently chosen. Practically it is better to have a relatively flat tipped rod, since a sharp rod may poke holes in the environmentally protective sheet material that is used over the metal horn aperture in practice. The terminal taper length is suggested to be half a free space wavelength by [76], yielding a length of 4.997 mm. In [76] the total length of the rod antenna is defined as being from the feed edge to half of the length of the terminal taper. To obtain the final physical length of the rod antenna, half the length of the terminal taper must therefore be added to the total length obtained earlier, giving a final physical length of 79.480 mm. With this, the stand alone rod antenna is completely defined.

4.5 Dimensions of antenna

Geometrical Parameters	Top radius (in mm)	Bottom radius (in mm)	Length (in mm)
Feed taper	1.8	3	15.396
Main body	1.8	1.8	61.586
Terminal taper	1	1.8	4.997

Table 4.1 Dimensions of antenna

4.6 Simulation results

Various electrical parameters are obtained by simulation by using the CST Microwave Studio at two different frequencies. Figure: 4.4 depict the s-parameters (S11 in dB) of the proposed antenna.

At frequency 29GHz the gain of the antenna is shown in Figure: 4.13, in principle E-and H-plane which is 17.23dB. The radiation efficiency is 66.99% and total efficiency is 66.83%.

At frequency 32.6GHz the gain of the antenna is shown in Fig. 4.16, in the principle E-and H-plane which is 14.36dB. The radiation efficiency is 74.21% and total efficiency is 73.70%. The E- and H-plane radiation patterns of the proposed antenna reveals high side-lobe levels, especially in the E-plane. This is about the only fundamental disadvantage of the dielectric rod antenna. However, some end-fire gain and main beam sharpness could be sacrificed to reduce the level of the side-lobes. The pattern bandwidth depends on the intended application of the antenna. Not knowing the surface wave excitation efficiency of the feed was the only difficulty, which have to encounter during the design process. The field near the rod is decomposed in to the guided and unguided wave. By using these two waves, feed and terminal pattern can be evaluated and by superposing the feed and terminal pattern of the dielectric rod antenna. The

technique of superposing the two patterns had the advantage that the gain of a long rod can be efficiently evaluated.

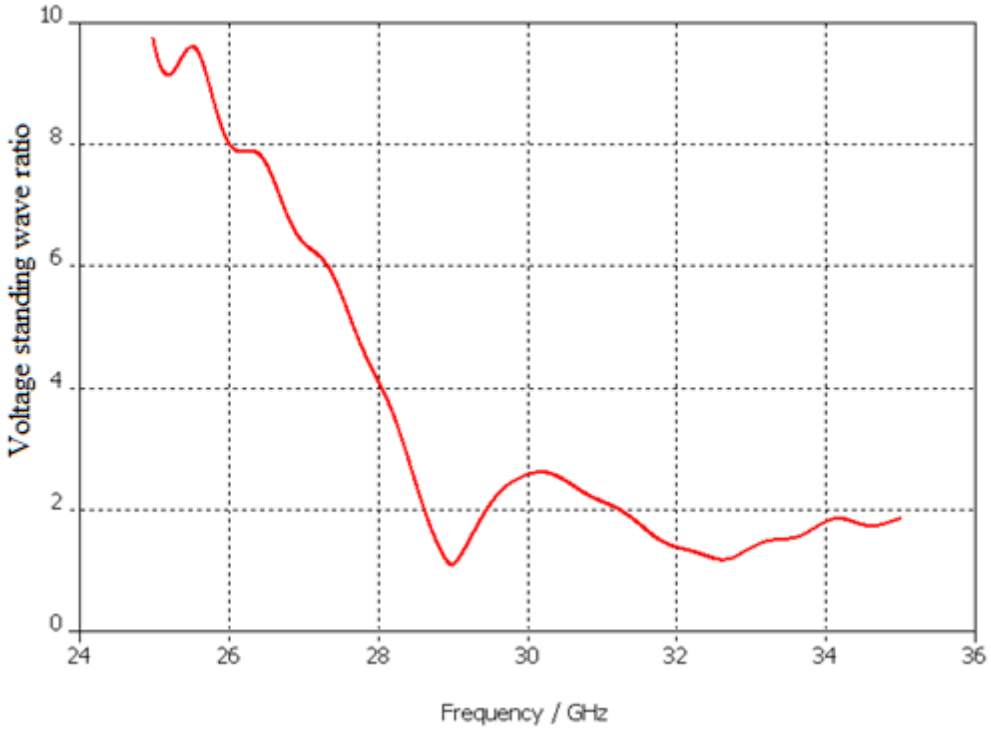

Figure: 4.3 VSWR curve of antenna

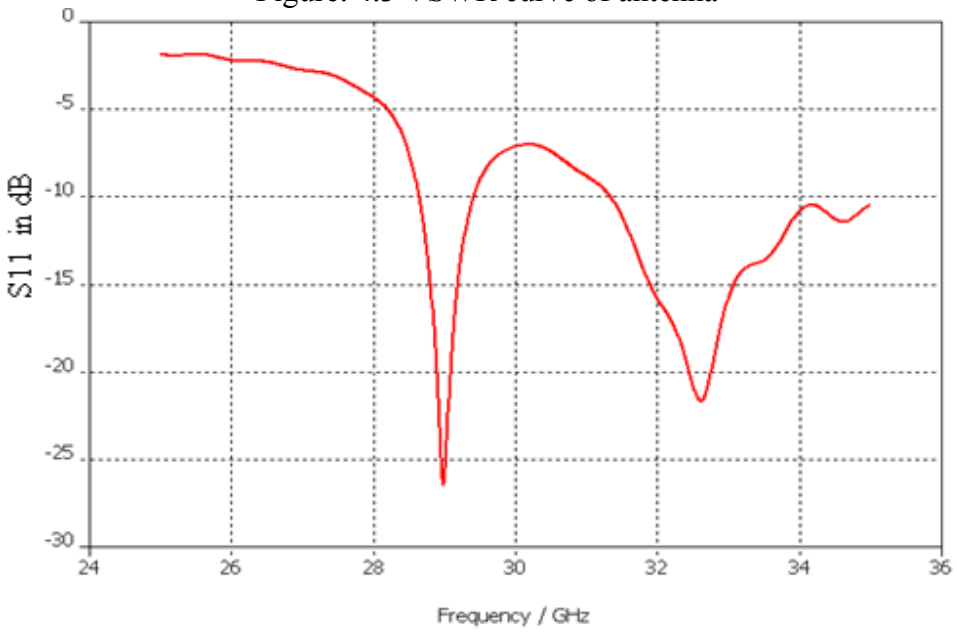

Figure: 4.4 Return loss characteristics of the dielectric rod antenna

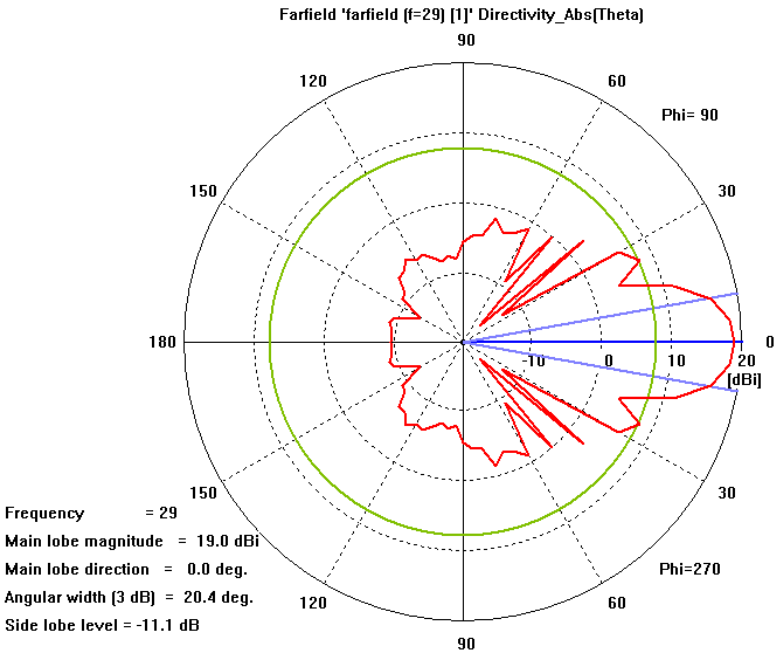

Figure: 4.5 polar plot directivity of antenna at 29 GHz

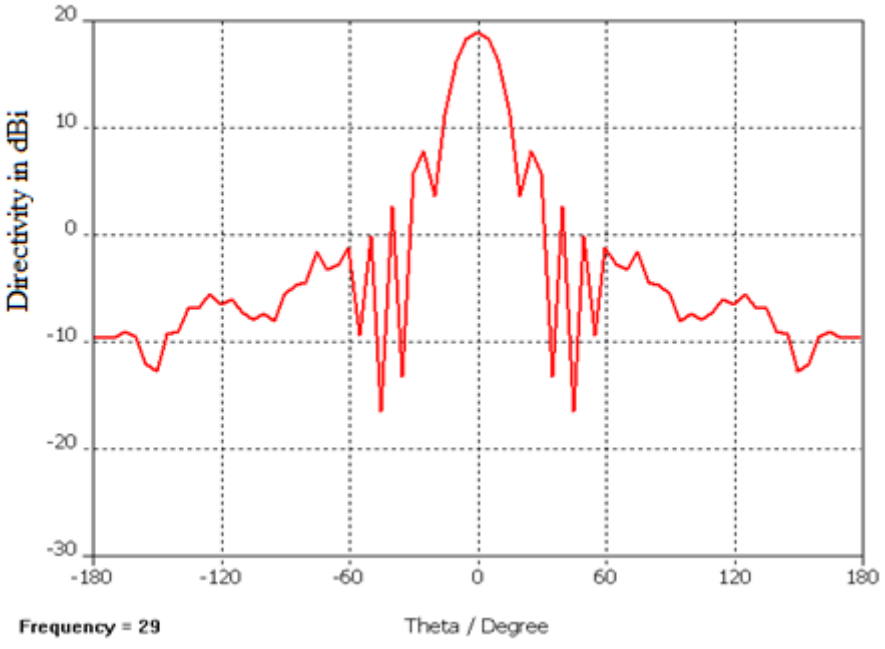

Figure: 4.6 Cartesian plot of directivity at 29 GHz

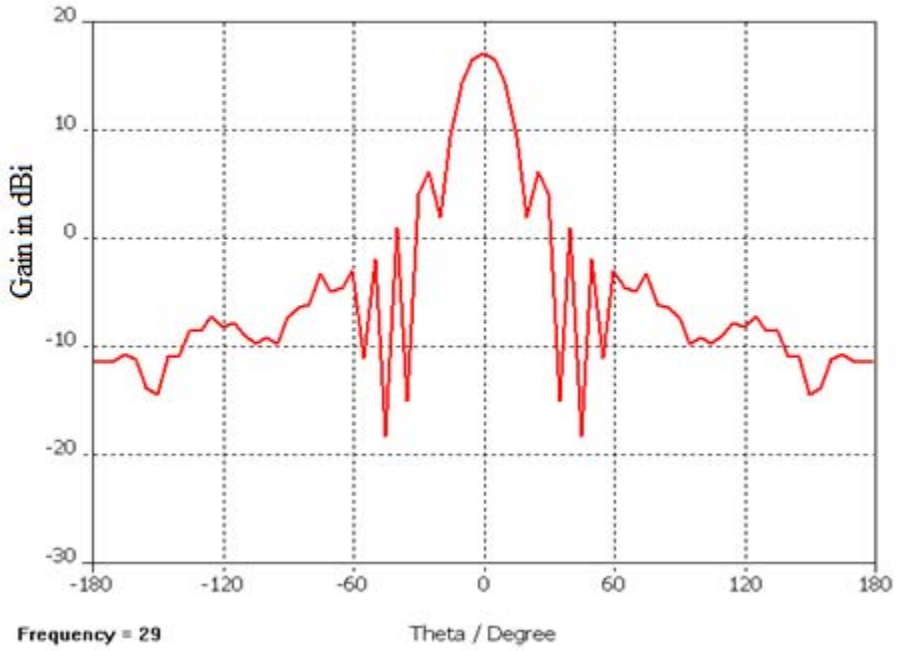

Figure: 4.7 Cartesian plot of gain at 29 GHz

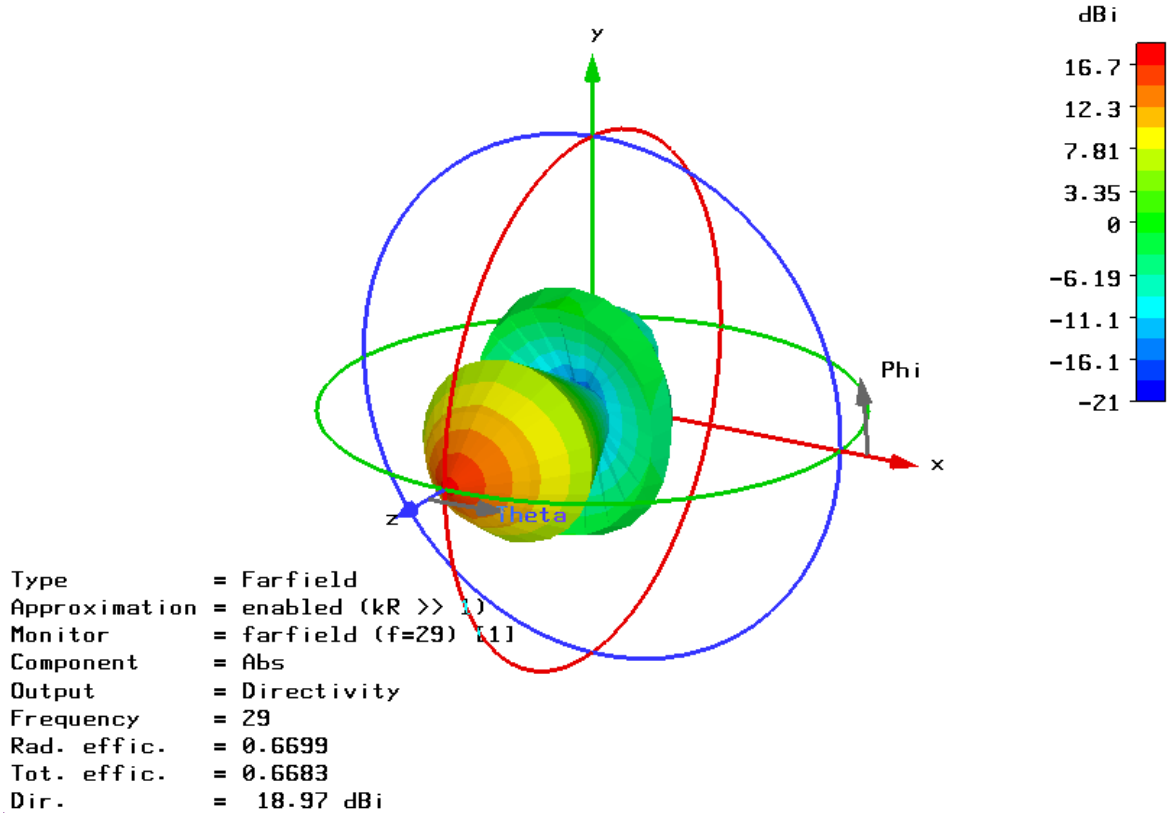

Figure: 4.8 3D plot of Directivity at 29 GHz

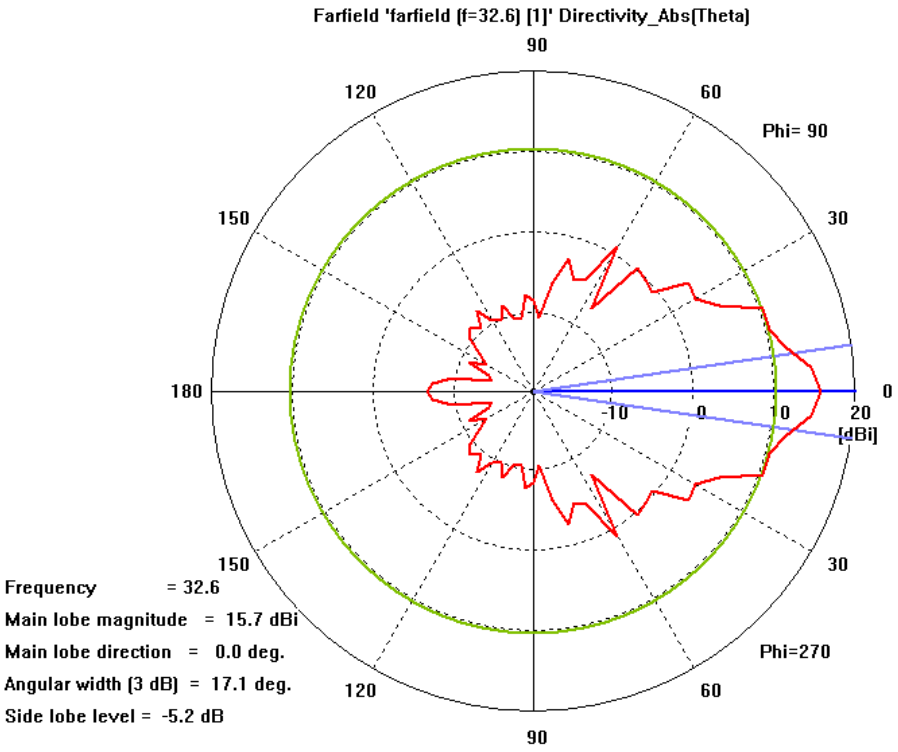

Figure: 4.9 polar plot of directivity at 32.6 GHz

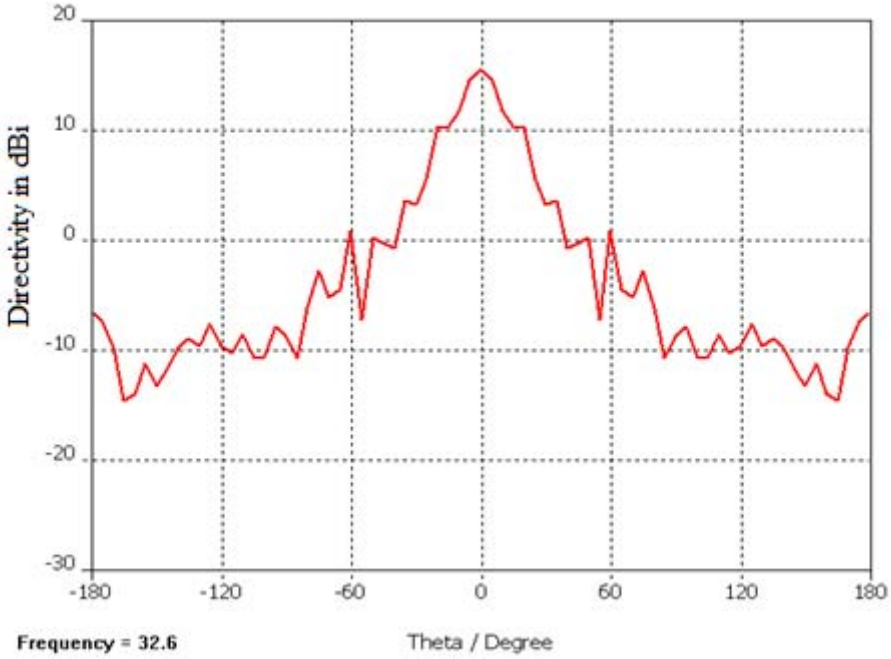

Figure: 4.10 Cartesian plot of directivity at 32.6 GHz

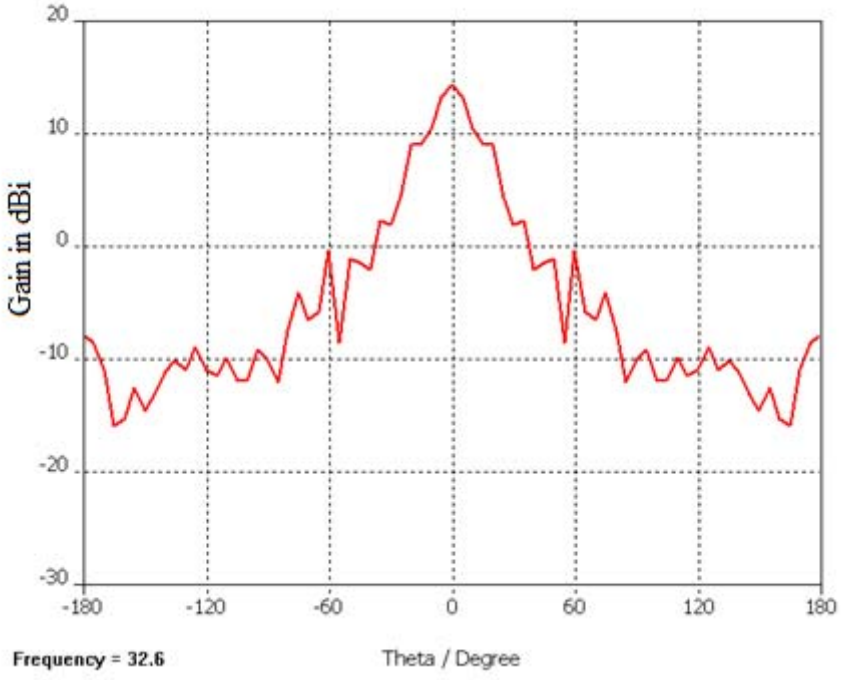

Figure: 4.11 Cartesian plot of gain at 32.6GHz

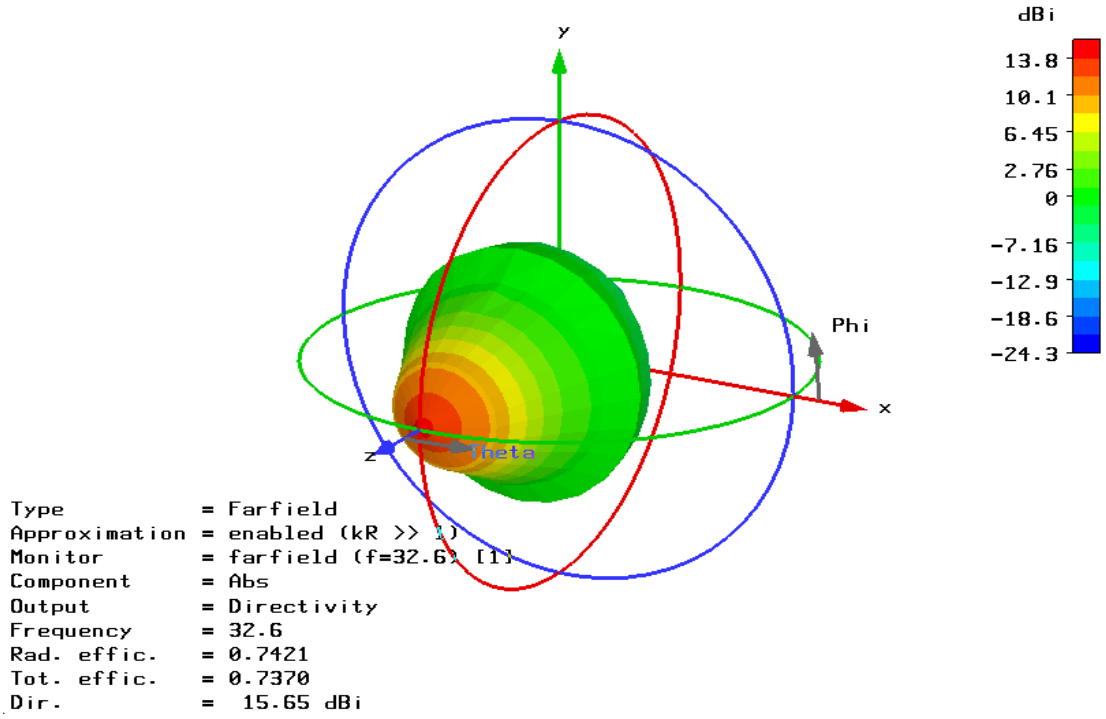

Figure: 4.12 3D plot of directivity at 32.6 GHz

2.6.1 Directivity and gain in E-and H-plane:

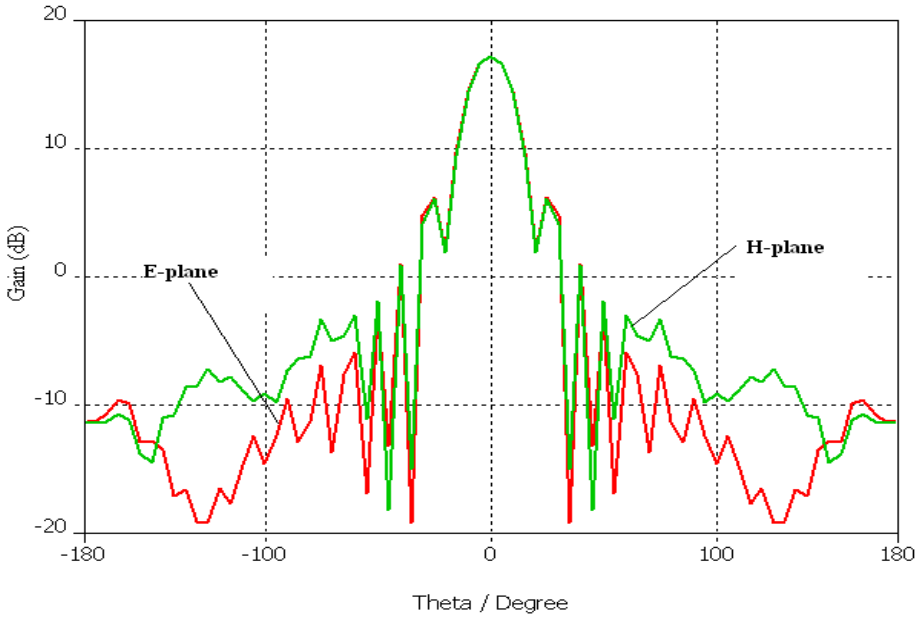

Figure: 4.13 Gain of antenna in E-plane and H-plane at 29 GHz

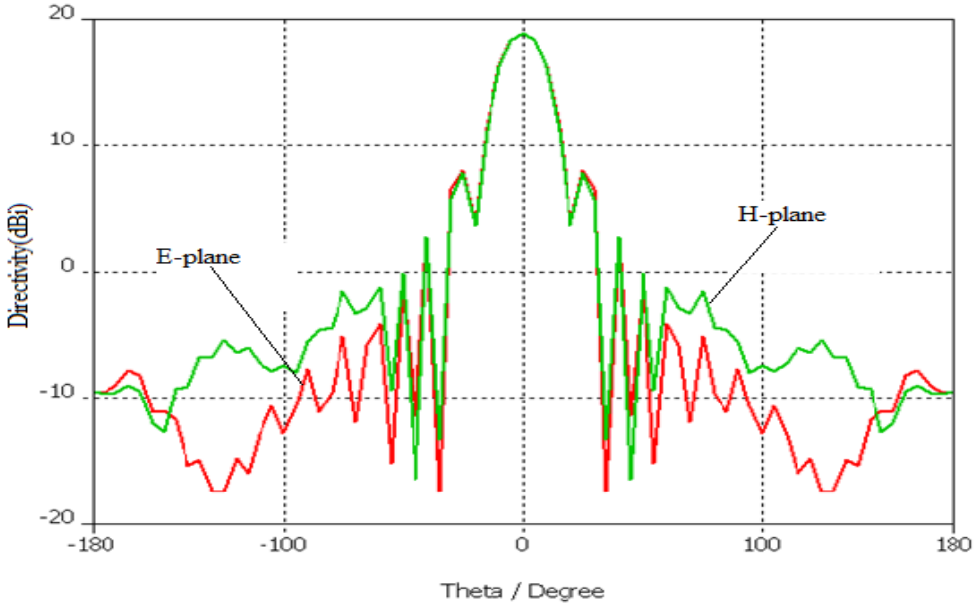

Figure: 4.14 directivity of antenna in E-plane and H-plane at 29GHz

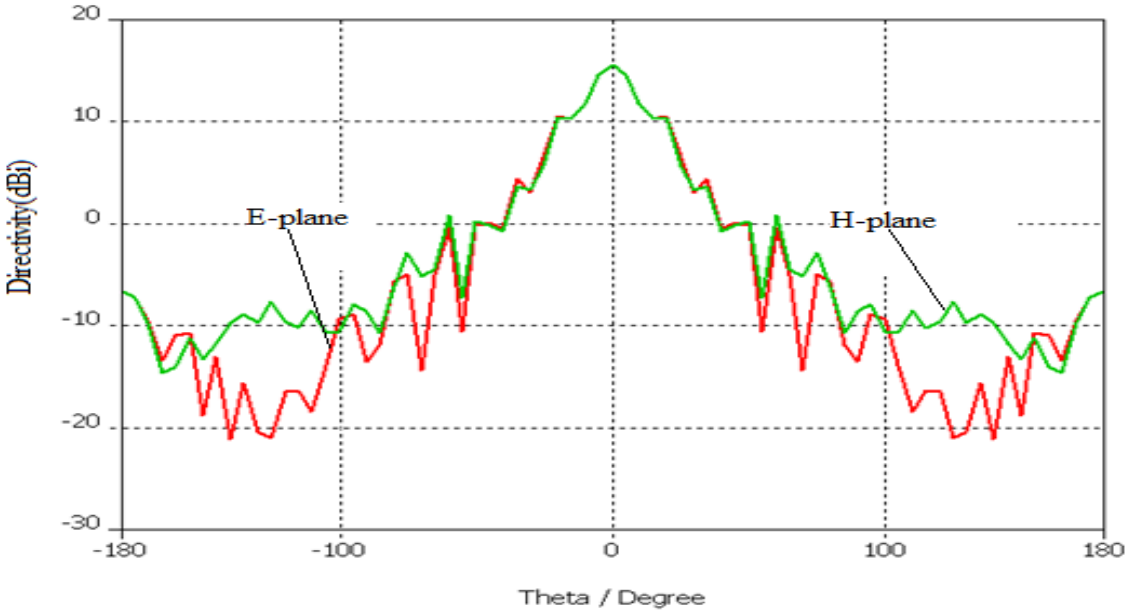

Figure: 4.15 Directivity of antenna E and H plane at 32.6 GHz

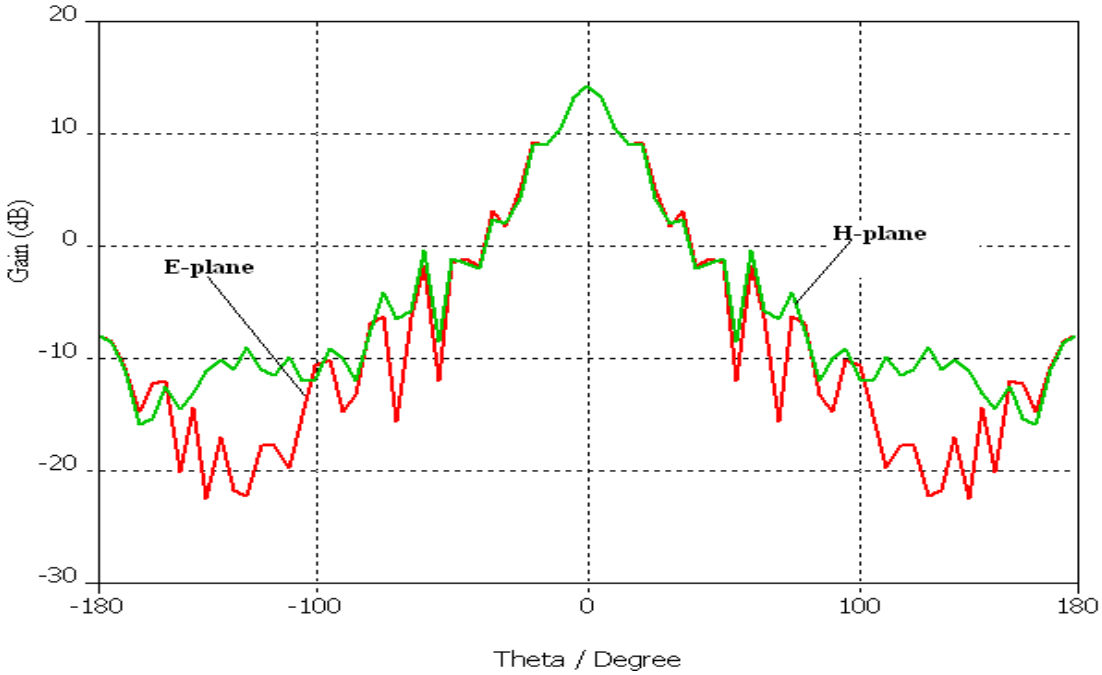

Figure: 4.16 Gain of antenna in E and H plane at 32.6GHz

Chapter 5

Conclusion

The objective of this project is to analytically study the Frequency Selective Surfaces and dielectric rod antenna and to use this Frequency Selective Surface to enhance the performance, particularly, gain and directivity of a high frequency antenna. Here we have studied various kinds frequency selective surfaces having shapes like circular, hexagonal, square, patch as well as loops, their designs and results using various research papers and books. We successfully redesigned them to work at the desired frequency range and analyzed and validated with simulation results like scattering parameters which described their bandpass or bandstop characteristics by using the CST Microwave Studio. To analyze the working of these surfaces, we proposed an equivalent circuit modeling technique in which an infinite array is represented by inductors and capacitors and this equivalent circuit is implemented by using the ANSOFT HFSS designer and the results from the ANSOFT are validated with the results of CST Microwave Studio. While working on these Frequency Selective Surfaces, we concluded that double square loop with patch is easy to design and have large bandwidth as compare to other surfaces.

In the next phase of our project, we have designed the dielectric rod antenna because the fabrication of this antenna is easy as compared to others. We designed the dielectric rod by using the CST and obtained the results of various parameters of an antenna like radiation pattern, radiation efficiency, s-parameters, gain, and directivity. After studying these parameters we concluded that this antenna provides good directivity, gain and we obtained multiple bands of operation.

In the future frequency Selective Surfaces can be used along with dielectric rod antenna to enhance its performance.

References

[1] T. K. Wu, Frequency Selective Surfaces and Grid Array. New York: John Wiley and Sons, Inc., 1995.

[2] C. C. Chen, Transmission through a conducting screen perforated periodically with apertures," IEEE Trans. Microwave Theory Tech., vol. 18, no. 9, pp. 627-632, 1970.

[3] C. Mias, C. Tsakonas, and C. Oswald, An investigation into the feasibility of designing frequency selective windows employing periodic structures (Ref. AY3922). Final report for the Radiocommunications Agency." Nottingham Trent University, Tech. Rep., 2001.

[4] G. Marconi and C.S. Franklin, "Reflector for use in wireless telegraphy and telephony", US Patent 1,301,473, April 1919.

[5] M. J. Archer, Wave reactance of thin planar strip gratings," Int. J. Electronics, vol. 58, no. 2, pp. 197-230, 1985.

[6] R. Collin, Field Theory of Guided Waves, 2nd ed. New York: IEEE Press, 1991.

[7]B. A. Munk, Frequency Selective Surfaces Theory and Design. New York: John Wiley and Sons, Inc., 2000.

[8] T. K. Wu, Frequency Selective Surfaces and Grid Array. New York: John Wiley and Sons, Inc., 1995.

[9] Y. Kasashima, Theoretical analysis of frequency selective shielding films," in Proc. EMC Zurich, 2001, pp. 5-10.

[10] P. Callaghan, E. A. Parker, and R. J. Langley, \Influence of supporting dielectric layers on the transmission properties of frequency selective surfaces," IEE Proc. H: Microw. Antennas Propag., vol. 138, no. 5, pp. 448{454, 1991.

[11] S. B. Savia and E. A. Parker, \Equivalent circuit model for superdense linear dipole FSS,"IEE Proc. | Microw. Antennas Propag., vol. 150, no. 1, pp. 37-42, 2003.

[12] R. Cahill and E.A. Parker, "Concentric ring and Jerusalem cross arrays as frequency selective surfaces for a 45° incidence diplexer". Electronics Letters, vol. 18, no. 17, April 1982, pp.313-314.

[13] S. M. A. Hamdy and E. A. Parker, Current distribution on the elements of a square loop frequency selective surface," Electron. Lett., vol. 18, no. 14, pp. 624-626, 1982.

[14] R. J. Langley and E. A. Parker, \Equivalent circuit model for arrays of square loops," electron. Lett., vol. 18, no. 7, pp. 294{296, 1982.

[15] Double-square frequency-selective surfaces and their equivalent circuit," Electron.Lett., vol. 19, no. 17, pp. 675-677, 1983.

[16] S. W. Lee, G. Zarrillo, and C. L. Law, Simple formulas for transmission through periodic metal grids or plates," IEEE Trans. Antennas Propagat., vol. AP-30, no. 5, pp. 904-909, 1982.

[17] A. D. Chuprin, E. A. Parker, and J. C. Batchelor, Convoluted double square: single layer FSS with close band spacings," Electron. Lett., vol. 36, no. 22, pp. 1830-1831, 2000.

[18] B. A. Munk, Transmission through a two-layer array of loaded slots," IEEE Trans.Antennas Propagate., vol. AP-22, no. 6, pp. 804-809, 1974.

[19] P. Callaghan and E. A. Parker, Tuning interactions of cascaded-frequency selective-slot arrays," IEE Proc. Microw. Antennas Propag., vol. 141, no. 4, pp. 290-294, 1994.

[20] C. K. Lee and R. J. Langley, Equivalent-circuit models for frequency-selective surfaces atoblique angles of incidence," IEE Proc. H, vol. 132, no. 6, pp. 395-399, 1985.

[21] P. T. Teo, X. F. Luo, and C. K. Lee, Transmission of convoluted periodic loop element with selective reflection," Appl. Phys. Lett., vol. 85, no. 9, pp. 1454-1456, 2004.

[22] E. A. Parker and A. N. A. El Sheikh, Convoluted array elements and reduced size unit cells for frequency-selective surfaces," IEE Proc. | H, vol. 138, no. 1, pp. 19-22, 1991.

[23] C. Antonopoulos and E. A. Parker, Design procedure for FSS with wide transmission band and rapid rolloff," IEE Proc. | Microw. Antennas Propag., vol. 145, no. 6, pp. 508{510, 1998.

[24] J. C. Vardaxoglou and D. Lockyer, \Modified FSS response from two sided and closely coupled arrays," Electron. Lett., vol. 30, no. 22, pp. 1818-1819, 1994.

[25] M. Hook and K. Ward, Passive FSS development and test report. Work package 3,"Culham Electromagnetics and Lightning Limited, Tech. Rep. Ofcom AY4462 project, 2004.

[26] N. Marcuvitz, Waveguide Handbook. New York: Peter Peregrinus Ltd., 1986, vol. 21.

[27] B. A. Munk, On stabilization of the bandwidth of a dichroic surface by use of dielectric slabs." Electromagnetics, vol. 5, no. 4, pp. 349-373, 1985.

[28] T. Larsen, A survey of the theory of wire grids," IRE Trans. Microwave Theory Tech,vol. 10, no. 3, pp. 191-201, 1962.

[29] Z. L. Wang, K. Hashimoto, N. Shinohara, and H. Matsumoto, Frequency-selective surface for microwave power transmission," IEEE Trans. Microwave Theory Tech., vol. 47, no. 10,pp. 2039-2042, 1999.

[30] R. J. Langley and A. J. Drinkwater, Improved empirical model for the Jerusalem cross,"IEE Proc. | H, vol. 129, no. 1, pp. 1-6, 1982.

[31] G. H. Sung, K. W. Sowerby, and A. G. Williamson, \Equivalent circuit modeling of a frequency selective plasterboard wall," in Proc. IEEE AP-S Int. Symp., vol. 4A,WashingtonD.C., 2005, pp. 400-403.

[32] |The impact of frequency selective surfaces applied to standard wall construction materials," in Proc. IEEE AP-S Int. Symp., vol. 2, Monterey, CA, 2004, pp. 2187-2190.

[33] |The angle dependent propagation characteristics of a frequency selective surface applied to plasterboard," in Proc. IEICE Int. Symp. on Antennas and Propagat., Sendai, Japan, 2004, pp. 1057-1060.

[34] I. Bardi, R. Remski, D. Perry, and Z. Cendes, Plane wave scattering from frequency-selective surfaces by the finite-element method," IEEE Trans. Magn., vol. 38, no. 2, pp. 641-644, 2002.

[35] K. Yee, Numerical solution of initial boundary value problems involving Maxwell's equations in isotropic media," IEEE Trans. Antennas Propagat., vol. 14, no. 3, pp. 302-307, 1966.

[36] A. Taflove and K. R. Umashankar, \The finite-difference time-domain (FDTD) method for numerical modeling of electromagnetic scattering," IEEE Trans. Magn., vol. 25, no. 4,pp. 3086-3091, 1989.

[37] R. Mittra, C. H. Chan, and T. Cwik, Techniques for analyzing frequency selective surfaces-a review," Proc. IEEE, vol. 76, no. 12, pp. 1593-1615, 1988.

[38] C. C. Chen, Transmission of microwave through perforated flat plates of finite thickness,"IEEE Trans. Microwave Theory Tech., vol. MTT21, no. 1, pp. 1-6, 1973.

[39] R. Paknys, \Reflection and transmission by reinforced concrete numerical and asymptotic analysis," IEEE Trans. Antennas Propagat., vol. 51, no. 10, pp. 2852-2861, 2003.

[40] D. S. Weile, E. Michielssen, and K. Gallivan, Reduced-order modeling of multiscreenfrequency-selective surfaces using Krylov-based rational interpolation," IEEE Trans. Antennas Propagat., vol. 49, no. 5, pp. 801-813, 2001.

[41] X. F. Luo, P. T. Teo, A. Qing, and C. K. Lee, \Design of double-square-loop frequency selective surfaces using differential evolution strategy coupled with equivalent-circuit model," Microwave Opt. Technol. Lett., vol. 44, no. 2, pp. 159-162, 2005.

[42]C. C. Chen, Transmission through a conducting screen perforated periodically with apertures," IEEE Trans. Microwave Theory Tech., vol. 18, no. 9, pp. 627-632, 1970. IEEE Trans. Antennas Propagat., vol. 49, no. 10, pp. 1470-1478, 2001.

[43] J. D'Angelo and I. D. Mayergoyz, Three dimensional RF scattering by the finite element method," IEEE Trans. Magn., vol. 27, no. 5, pp. 3827-3832, 1991.

[44] M. Hara, T. Wada, T. Fukasawa, and F. Kikuchi, \A three dimensional analysis of RF electromagnetic fields by the finite element method," IEEE Trans. Magn., vol. 19, no. 6, pp. 2417-2420, 1983.

[45] T. F. Eibert, Y. E. Erdemli, and J. L. Volakis, Hybrid finite element-fast spectral domain multilayer boundary integral modeling of doubly periodic structures," IEEE Trans. Antennas Propagat., vol. 51, no. 9, pp. 2517-2520, 2003.

[46] E. A. Parker, A. D. Chuprin, and R. J. Langley, \Finite element analysis of electromagnetic wave diffraction from buildings incorporating frequency selective walls," IEE Proc. Microw. Antennas Propag., vol. 146, no. 5, pp. 319-323, 1999.

[47] M. Jayawardene, R. Dickie, J. A. Flint, J. C. Vardaxoglou, R. Cahill, H. S. Gamble, V. F.Fusco, and N. Grant, Multilayer aperture ring frequency selective surface modelling," in Proc. IEEE AP-S Int. Symp., vol. 4A, Washington D.C., 2005, pp. 392-395.

[48] Z. Lou and L. M. Jin, High-order finite-element analysis of electromagnetic scattering from periodic structures," in Proc. IEEE AP-S Int. Symp., vol. 2, 2003, pp. 153-156.

[49] J. Jin, The Finite Element Method in Electromagnetics. New York: John Wiley and Sons, 1993.

[50] A. Taflove and S. Hagness, Computational electrodynamics : the finite-difference time-domain method., 2nd ed., ser. Artech House antennas and propagation library. Boston,MA: Boston, MA : Artech House, 2000., 2000.

[51] http://en.wikipedia.org/wiki/FDTD, (as seen on 02/Feb/2010).

[52] A. Taflove and K. R. Umashankar, Review of FDTD numerical modeling of electromagnetic wave scattering and radar cross section," Proc. IEEE, vol. 77, no. 5, pp. 682-699, 1989.

[53] P. Harms, R. Mittra, and W. Ko, Implementation of the periodic boundary condition in the finite-difference time-domain algorithm for FSS structures," IEEE Trans. Antennas Propagat., vol. 42, no. 9, pp. 1317-1324, 1994.

[54] Y. A. Kao and R. Atkins, A finite difference-time domain approach for frequency selective surfaces at oblique incidence," in Proc. IEEE AP-S Int. Symp., vol. 2, 1996, pp. 1432-1435.

[55] W. Yu, S. Dey, and R. Mittra, Modeling of periodic structures using the finite difference time domain (FDTD)," in Proc. IEEE AP-S Int. Symp., vol. 1, 1999, pp. 594-597 vol.1.

[56] L. W. Henderson, The scattering of planner array of arbitrary shaped slot and/or wire elements in a stratified dielectric medium," Ph.D. dissertation, Ohio State University, 1983.

[57] B. Monacelli, G. Boreman, J. Pryor, B. A. Munk, and D. Kotter, \Infrared frequency selective surfaces," in Proc. IEEE AP-S Int. Symp., vol. 2, Monterey, CA, 2004, pp. 2175{2178.

[58] J. Blackburn and L. R. Arnaut, \Numerical convergence in periodic method of moments analysis of frequency-selective surfaces based on wire elements," IEEE Trans. Antennas Propagat., vol. 53, no. 10, pp. 3308{3315, 2005.

[59] D. S.Weile and E. Michielssen, Analysis of frequency selective surfaces through the blazingonset using rational Krylov model-order reduction and Woodbury singularity extraction,"

[60] C. Mias, \Frequency selective absorption using lumped element frequency selective surfaces," Electron. Lett., vol. 39, no. 11, pp. 847-849, 2003.

[61]. ANDERSON, I.: 'On the theory of self-resonant grids', Bell Syst. Tech. J., 1975, 54, pp. 1725-1731

[62]. T. K. Wu, Frequency Selective Surfaces and Grid Array. New York: John Wiley and Sons, Inc., 1995.

[63]. S. M. A. Hamdy and E. A. Parker, “Current distribution on the elements of a square loop frequency selective surface," Electron. Lett., vol. 18, no. 14, pp. 624-626, 1982.

[64]. R. J. Langley and E. A. Parker, “Equivalent circuit model for arrays of square loops,"Electron. Lett., vol. 18, no. 7, pp. 294-296, 1982.

[65].C. K. Lee and R. J. Langley, “Equivalent-circuit models for frequency-selective surfaces at oblique angles of incidence," IEE Proc.| H, vol. 132, no. 6, pp. 395-399, 1985.

[66]. M. J. Archer, \Wave reactance of thin planar strip gratings," Int. J. Electronics, vol. 58,no. 2, pp. 197-230, 1985.

[67]. N. Marcuvitz, Waveguide Handbook. New York: Peter Peregrinus Ltd., 1986, vol. 21.

[68].DOUBLE-SQUARE FREQUENCY-SELECTIVE SURFACES AND THEIR EQUIVALENT CIRCUIT ,R. J. LANGLEY E. A. PARKER The Electronics Laboratories The University Canterbury, Kent CT2 7NT, England,30th June 1983

[69] "Croation Vodatel and SES ASTRA Introduce Broadband Internet and Video On Demand Services", press release of SES-ASTRA 10 January 2005, www.ses-astra.com/press-info/news/press-re1eases105120050110.shtm1.

[70] "About EMS SatNet", Company Information for EMS Satellite Networks, www.emssatnet.com/companyinfo.asp.

[71] "Broadband Satellite Communications", presentation of DC-SAT.NET LTD,www.dc-sat.net, http:lldc-sat.netlpdfs/DC%2OBroadband%2OSate1lite%2OCommunications.pdf.

[72] "Satellite Internet Services", Broadband Products and Services from SES-ASTRA, www.ses-astra.com/products/broadband/sis.shtml

[73] Astra Return Channel System ARCS SIT, Schedule L-Outdoor Unit Specification,Doc.No. ARCS.25C.CT-A001-3.0, 13 December 1998.

[75] ETSI EN 301 359 V1.l.l (1999-04), " Satellite Earth Stations and Systems (SES);Satellite Interactive Terminals (SIT) using satellites in geostationary orbit operating in the 11 GHz to 12 GHz (space-to-earth) and 29.5 GHz to 30.0 GHz (earth-tospace) frequency bands.

[76] R.C. Johnson and H. Jasik, "Antenna Engineering Handbook", 2nd edition, Chapter 12, F.J Zucker, McGraw-Hill, 1984